GPNMB+ microglia moderate the amyloid beta-tau interaction in early Alzheimer's disease

Akihiro Kitani[1], Yusuke Matsui[1,2]

[1]Biomedical and Health Informatics Unit, Department of Integrated Health Science, Nagoya University Graduate School of Medicine, Nagoya, Japan

[2]Institute for Glyco-core Research (iGCORE), Nagoya University, 461-8673 Nagoya, Aichi, Japan.

Corresponding author

Yusuke Matsui

E-mail: matsui@met.nagoya-u.ac.jp

Summary

Although interactions between amyloid-beta (Aβ) and tau proteins have been implicated in Alzheimer's disease (AD), the detailed mechanisms by which these interactions contribute to disease progression remain unclear. In this study, we evaluated proteomics and protein–protein interaction data using BIONC, a deep learning-based network integration method to investigate factors moderating the effects of the Aβ-tau interaction in mild cognitive impairment and early-stage AD. Our results suggested that astrocytes and GPNMB+ microglia moderate the Aβ-tau interaction. Based on linear regression with histopathological and gene expression data, GFAP and IBA1 levels and *GPNMB* gene expression positively contributed to the interaction of tau with Aβ in non-dementia cases, replicating the results of the network analysis. These findings indicate that GPNMB+ microglia moderate the Aβ-tau interaction in early AD and therefore are a novel therapeutic target.

Keywords

Alzheimer’s disease, Tau, Amyloid β, microglia, astrocyte, GPNMB, proteomics, network integration, moderator, interaction effects

Introduction

Alzheimer's disease (AD) is the most common form of dementia, characterized by extracellular amyloid-beta (Aβ) plaques and intracellular tau protein tangles, which are believed to be central to its pathology.[1–3] Recent studies have reported an interaction between Aβ and tau proteins in the pathogenesis of AD, contributing to disease progression.[4–8] For instance, Lee et al.[7] revealed that Aβ-tau interactions are associated with the propagation of tau. In practice, lecanemab, an anti-Aβ antibody, which has been shown to slow cognitive decline in patients with early-stage AD, reduces total tau protein and P-Tau181 levels in cerebrospinal fluid.[9] This suggests that Aβ contributes to the effect of tau in AD. Moreover, several phenotypes are associated with the Aβ-tau interaction, such as astrocyte reactivity, blood pressure, vascular burden, and microglia;[10–13] however, the detailed mechanisms are not fully understood. Various cellular perturbations have been identified through single-nucleus RNA sequencing (snRNA-seq) in AD.[14–20] For example, recent snRNA-seq study[15] have revealed the presence of Trem2-dependent disease-associated microglia (DAM) and a unique Serpina3n+C4b+ reactive oligodendrocyte population in 5XFAD mice. In human AD, distinct glial phenotypes include *IRF8*-driven reactive microglia and oligodendrocytes with impaired myelination and metabolic adaptation to neuronal degeneration have been observed. However, the specific cell types and effects of Aβ-tau interactions have yet to be elucidated.

Network analyses based on gene or protein co-expression have revealed gene groups

and associated pathways correlated with pathological and clinical factors in AD.[21–23] Additionally, network integration methods based on multi-omics and other data types have been developed.[24–27] By considering both physical and functional interactions simultaneously, network integration analyses can identify detailed molecular relationships. However, this approach has largely been applied to cancer. AD is a complex disease involving various pathologies, and network integration is a promising approach for determining comprehensive physical and functional interactions involving Aβ and tau in AD.

In this study, we investigated moderating factors in the Aβ-tau interaction using a systematic network integration approach. The aim of this study was to elucidate the cell types and moderating factors in the interaction between Aβ and tau proteins in early-stage AD. In particular, we investigated the moderating factors using BIONIC,[28] a network integration algorithm and linear regression with histopathological data. In the integrated network, glial cell-related proteins, including those associated with microglia and astrocytes, were enriched around *APP* and *MAPT* subnetworks, which encode the precursors of Aβ and Tau, respectively. Further analyses of microglial subtypes revealed enrichment in GPNMB+ microglia. Additionally, a linear regression analysis based on histopathological and gene expression data showed that interactions between Aβ and various markers, such as IBA1, GFAP, and *GPNMB*, were positively related to tau levels. These results suggest that astrocytes and GPNMB+ microglia are involved in the Aβ-tau interaction in early-stage AD, providing a basis for the development of more effective treatments.

70

Results

Study design

The analysis workflow, including an overview of the datasets, methods, and results, is presented in Figure S1. We extracted proteomics data for patients with mild cognitive impairment (MCI) or early-stage AD and healthy individuals, constructed a co-expression network, and integrated this network with a protein–protein interaction (PPI) network. To characterize the integrated data, we utilized whole snRNA-seq data (Figure 1). Using proteomics data, we searched for factors associated with tau and Aβ (Figure 2), constructed a subnetwork of tau, Aβ, and moderators, and performed cell type and functional enrichment analyses (Figure 3). We validated these findings using immunohistochemical data from a separate cohort (Figure 4). Additionally, for the subnetworks, we obtained microglia-specific snRNA-seq data to perform a microglial cell subtype enrichment analysis (Figure 5). Finally, we again validated these findings using immunohistochemical and gene expression data (Figure 6).

Integration of protein co-expression and physical protein–protein interaction networks

We constructed an integrated network as a basis for analyzing the effects of PPIs and their moderators in the AD postmortem brain. To this end, we integrated proteomic data and a physical PPI network to construct a functional-physical PPI network. We employed BIONIC,[28] which was designed to integrate multiple biological networks, while preserving the integrity of

each individual network using deep learning[29] (Figure 1A). BIONIC uses a graph attention network to integrate multiple networks, maintain the distinctive characteristics of each network, generate new features, and construct networks. It shows good performance[28] and has been used in analyses of gene interactions in cancer.[30]

First, a functional protein interaction network was constructed based on protein abundance data. We compiled postmortem proteome profiles for patients with MCI and early-stage AD from the dorsolateral prefrontal cortex (DLPFC), which were available from the Religious Order Study (ROS) and Rush Memory and Aging Project (MAP) cohort (https://adknowledgeportal.synapse.org/). Next, we generated a PPI network using the STRING database[31](https://string-db.org/) and constructed sub-networks by prioritizing "high confidence" interactions. Using BIONIC, the integrated network was embedded into a lower-dimensional vector space, and the embedded coordinates were obtained in a 512-dimensional space. Our downstream analysis used 512 integrated network features.

Characterizing integrated protein network modules

Next, we characterized the biological context captured by the integrated network. In particular, we evaluated cell types and biological functions associated with the protein modules in the integrated network. To investigate the protein network modules, we built k-nearest neighbor graphs of proteins based on the integrated network to obtain clusters (see Methods and Figures

1A and B). The cell types and biological processes corresponding to each module were inferred. The modules in the integrated network contained cell type signatures (Figure 1C) and were enriched in biological processes related to these cell types (Supplementary Table S1 and Figure 1D). For example, module 1 was characterized by endothelial cells, microglia, and astrocytes, modules 5, 17, 22, and 27 were associated with oligodendrocytes, modules 9 and 13 with astrocytes, and module 11 with neurons (Figure 1C). Consistent with the cell type results, in module 5, terms related to oligodendrocytes, such as “Ensheathment of neuron” and “Oligodendrocyte differentiation,” were identified, while module 11 was predominantly enriched in synapse-related terms (Figure 1D).

Identification of *APP* and *MAPT* as adjacent modules in the integrated network

We explored the relationships among modules within the integrated network. We specifically examined modules that included *APP* and *MAPT*, which serve as markers for amyloid-beta and tau, respectively. The *APP* gene was located in module 11, and *MAPT* was located in module 12. Additionally, *APOE*, which plays a significant role in the accumulation and aggregation of amyloid beta, was assigned to module 1. We then constructed a network of module–module interactions (See Methods) (Figure 1E and Figure S2). Notably, these three modules were in close proximity in the network, with a strong correlation between the *APP* and *MAPT* modules (Pearson correlation coefficient = 0.7667, $p < 0.001$). Additionally, strong

correlations were observed between the *APOE* module and both the *APP* (r = 0.6479, $p < 0.001$) and *MAPT* modules (r = 0.6289, $p < 0.001$). Furthermore, within the network, the *MAPT* module was closest to the *APP* module based on Euclidean distances; conversely, the *APP* module was second closest to the *MAPT* module. This module-to-module correlations in early-stage AD support the interactions between *APOE*, *APP*, and *MAPT*.[32,33]

Next, we evaluated whether similar findings could be obtained without network integration. Employing the STRING database with settings for high confidence and physical interactions alone, no interactions were detected between the *APP* and *MAPT* modules. Similarly, *APOE* did not interact with the other genes (Figure S3). Additionally, when examining protein expression data separately, *APP* and *MAPT* did not show significant correlations (Pearson's correlation coefficient = -0.0465, p = 0.61). These results underscore the importance of our integrated network approach in capturing the biological interactions between Aβ and tau, which are crucial for understanding early-stage AD development.

Stress response factors moderate amyloid β-tau interactions

Next, we aimed to identify factors that could moderate the Aβ-Tau interaction based on the integrated network. For this purpose, we prioritized proteins with strong moderating effects on APP-MAPT interactions against proteins close to the *APP* and *MAPT* modules. We utilized the computational framework of MINDy[34] (Modulator Inference by Network Dynamics) (Figure 2A). Briefly, MINDy calculates mutual information for interaction pairs (i.e., *APP* and *MAPT*),

conditioned by the expression of the modulator, which reflects the modulating effect. In the present analysis, we extracted the neighboring proteins of the *APP* and *MAPT* modules in the integrated network (see Methods). We then stratified the samples from the proteomics dataset into groups representing the top and bottom 35% of expression for each neighboring protein and evaluated differences in the magnitude of mutual information between *APP* and *MAPT* (Figure 2A). We analyzed 312 neighboring proteins and identified the 11 most significant modulators (Figure 2B). These candidates included factors involved in the cellular stress response (*HSPD1* and *HSPA5*),[35] ubiquitin-proteasome system (*USP48*, *KBTBD6*, *UBE2D4*, and *STAMBPL1*),[36–38] and apoptosis and cellular responses (*MAP3K5*).[38] These results suggest that proteostasis including stress response genes are related to the Aβ-tau interaction.

To further identify proteins contributing to the Aβ-tau interaction from the moderator candidates, we integrated proteins known to physically interact with Aβ and/or tau sourced from the Amyloidome[39] and Tau Interactome.[40] Heat Shock Protein Family A (Hsp70) Member 5 (*HSPA5*) was identified. *HSPA5*, a marker of ER stress associated with AD,[41,42] has been shown to interact in vitro with Aβ and tau, mitigating their toxicity.[43–47] Although in vivo studies have identified it as a candidate therapeutic target[48,49], the detailed mechanisms of action and its relevance in the Aβ-tau interaction are not fully understood.[50]

Glial cells are closely related to the APP-MAPT interaction in the integrated network

We further investigated whether stress responses involving *HSPA5* are involved in Aβ-tau interactions and identified related cell types and biological pathways. To address this, we exploited the integrated network extensively and reconstructed *HSPA5* and its neighboring subnetworks as well as *APP* and *MAPT* (Figure 3A). Note that the subnetwork included other significant moderators, *STAMBPL1* and *MAP3K5*, suggesting that these factors, in addition to *HSPA5*, could be associated with the Aβ-tau interaction. This subnetwork was characterized by functions in neuronal death, positive regulation of kinase activity, cellular response to chemical stress, synapse organization, and regulation of autophagy, confirming that it was related to stress response pathways (Figure 3B, see also Supplementary Table S2).

We classified proteins in the subnetwork into six communities based on topology and then estimated the cell types and biological functions associated with each community (Figure 3C, D, and Supplementary Table S3). We found that glial cells were the primary cell type related to the stress response subnetwork (Figure 3C). Additionally, the combined score for each community, calculated by multiplying the expression level by the proportion of cells, showed enrichment for glial cells (Figure S4A). Similar results were obtained using snRNA-seq data from two different cohorts[19,20] and different regions (Figures S4B and C). However, communities 2 and 6 were excluded from this analysis owing to the small number of genes included. In the APP-related community 3, oligodendrocytes were enriched in protein folding, oxidative stress responses,

neuronal death, and autophagy. Community 4, which contained *MAPT* and *HSPA5*, was characterized by microglia and excitatory neurons with enrichment in kinase activity. Other communities such as community 1 and 5 were also enriched in glial cells (Figure 3C and D). Microglia were detected as a feature of three of the four significantly enriched submodules (Figure 3C).

Histopathological data analysis validated the roles of microglia and astrocytes in the Aβ-tau interaction in early Alzheimer's disease

To further examine the effect of the interaction between Aβ and tau, we examined publicly available histopathological (ACT study) data.[51] This dataset contains extensive multimodal histopathological information, including Aβ and tau pathology. The distributions of age, sex, CERAD score, and Braak score in groups with and without dementia are shown in Figure S5. Among these parameters, CERAD and Braak scores showed significant differences between the groups (Fisher's exact test, $p = 0.00237$ and $p = 0.000468$, respectively). In the no-dementia group, the average CERAD score was 1.476 and the average Braak score was 3.421. Braak stages I and II indicate that neurofibrillary tangles are confined mainly to the entorhinal region of the brain, whereas stages III and IV involve the limbic regions, such as the hippocampus.

We analyzed the effect of the interaction between tau and Aβ using a linear modeling approach. We used Tau2, a antibody for a mature neurofibrillary tangles and dystrophic neurites,

as the dependent variable and Aβ along with GFAP or IBA1 (activated astrocyte or microglia markers, respectively) as independent variables. We investigated the interaction between GFAP or IBA1 and Aβ, stratifying the analysis by the dementia status and across four brain regions (Figure 4). For GFAP, a significant positive contribution to the interaction was observed in both dementia and no-dementia groups in the hippocampus (HIP, $\beta = 43.59$, $p = 0.022$ and $\beta = 24.852$ and $p = 0.001$, respectively) and in the no-dementia group in the temporal neocortex (TCx, $\beta = 4.352$ and $p < 0.001$). In the case of IBA1, there was a trend towards a positive contribution in the no-dementia group in the HIP, though the relationship was not significant ($\beta = 4.678$ and $p = 0.338$), and a significant positive contribution in the TCx ($\beta = 4.351$ and $p < 0.001$). Conversely, in the dementia group, a significant negative contribution was noted in the TCx (Figure 4B, $\beta = -11.124$, $p = 0.04$ and Supplementary Table S4). Analyses of AT8, an antibody that recognizes phospho-Tau (Ser202, Thr205) showed the same trend in the no-dementia group (GFAP, $\beta = 33.912$, $p = 0.198$ and $\beta = 62.732$, $p = 0.002$ in HIP and TCx, IBA1, $\beta = 14.442$, $p = 0.36$ and $\beta = 16.344$, $p < 0.001$, Supplementary Table S5). Of note, interactions were observed only in the HIP and TCx regions, which are vulnerable in patients with early-stage AD.[52]

These results suggest that the no-dementia group, although not exhibiting dementia, exhibited the mild progression of AD (Figures S5C and D). These results supported the hypothesis that astrocytes and microglia moderate the Aβ-tau interaction in early-stage AD.

GPNMB+ microglia function as moderators of the Aβ-tau interaction

We further examined microglial subtypes that contribute to Aβ-tau interactions. Microglia-overexpressing neuroinflammation-related processes can be assigned to subtypes that exhibit different cellular states under different AD conditions.[53] We evaluated whether a certain subtype of microglia moderates the Aβ-tau interaction in early-stage AD. We accessed recently reported snRNA-seq data[20] from frontal cortex biopsies of 52 patients with hydrocephalus (NPH). This cohort included samples with confirmed amyloid and tau pathologies, in which AD was in an asymptomatic stage. Of the 52 living biopsies, Aβ plaques were identified in 19 subjects, Aβ plaques and phosphorylated tau pathology in 8 subjects, and no pathology in the remaining 25 subjects; for subjects with Aβ pathology, the subsequent onset of AD was determined in longitudinal studies. In total, 892,828 high-quality single-nucleus profiles were included in analyses. We focused on the microglial cell populations.

We performed an enrichment analysis of each microglial subtype for the stress response-related subnetwork communities (communities 1–6) based on the integrated network. GPNMB+ microglia were significantly enriched in community 1 (Figure 5). The expression level and proportion of cells identified as the GPNMB+ microglial subtype were high for the community 1 signature score (Figure 5A). In addition, we compared the compositions of cell subtypes across different statuses in the same cohort. The frequency of GPNMB+ microglia was significantly higher in Aβ+ and Aβ+Tau+ samples than in the control group (Figure S6 and Supplementary

Table S6). The combined score for Community 1, calculated by multiplying the expression level and the proportion of cells with positive expression, further confirmed that the GPNMB+ microglial subtype was the highest ranked among the examined subtypes (Figure 5B). Importantly, the GPNMB+ microglial subtype is expressed in the early stages of AD and expands as the disease progresses.[20]

To further validate the involvement of GPNMB+ microglia in the Aβ-tau interaction in early-stage AD, we used another large-scale snRNA-seq data set for microglia subtypes in AD,[19] including transcriptome data for 194,000 single-nuclear microglia and multiple AD pathological phenotypes in 443 human subjects. The cell subtypes were annotated based on a previous study.[20] We found the same trend towards enrichment for GPNMB+ in Module 1 (Figure 5C and D). These results suggest that the stress response module moderating Aβ-tau interactions in early AD corresponds to GPNMB+ microglia.

Aβ-tau stress response mediators are activated prior to GPMNB+ microglial activation

We further examined the relationship between stress response-related mediators of the Aβ-tau interaction and GPNMB+ microglia. Previous studies have reported that ER stress induces GPNMB expression in neurons but not in microglia.[54] We hypothesized that stress response mediators are involved in the transition of microglia from a homeostatic state to an activated GPNMB+ state in the human brain. To test this hypothesis, trajectory analysis of the two

snRNA-seq datasets used in the previous analyses was performed using Slingshot.[55] Briefly, in this analysis, cells are embedded in the manifold space based on expression similarity between cells. This trajectory reflects the cellular state and can be treated as a “pseudo-time” axis. Multiple branched trajectories were identified. For each trajectory, we identified the GPNMB+ microglial coordinates on the pseudo-time trajectories (Figures S7A and C).

Next, we analyzed the points at which the candidate Aβ-tau-moderating factors related to the stress response predicted using MINDy were expressed in the pseudo-time analysis. In both datasets, the moderator proteins were highly expressed prior to GPNMB+ microglia in all pseudo-time trajectories (Figure S7B and D). Similar results were obtained for *HSPA5*, a moderating factor based on the amyloidome (i.e., the collection of amyloid peptides and related proteins, peptides, and other molecules)[39] and tau interactome. These results suggest that stress factors moderating the Aβ-tau interaction may act through the activation of GPNMB+ microglia.

GPMNB protein expression is correlated with the clinical severity of AD

We evaluated the hypothesis that GPMNB+ microglia drive Aβ-tau interactions in early AD. In particular, we examined whether *GPMNB* could serve as a biomarker for the clinical severity of AD.

For this purpose, we assessed brain tissue protein expression and clinical parameters from the ROSMAP cohort data using CERAD and Braak scores as indicators of the clinical

severity of AD. We stratified the patients into two groups based on *GPNMB* protein expression: the top 35% and bottom 35%. The *GPNMB* high- and low-expression groups corresponded to the GPNMB+ microglia-activated and non-activated groups, respectively. Within the ROSMAP cohort, the CERAD score is a semi-quantitative measure of neuritic plaques, where 1 indicates definite AD, 2 is probable AD, 3 is possible AD, and 4 represents no AD. The top 35% showed greater disease progression based on both CERAD and Braak scores than that of the bottom 35% (Figures 6A, B).

GPNMB shows significant Aβ-tau interaction effects in the preclinical stage

We further examined whether *GPNMB* moderates the effect of the Aβ-tau interaction in early-stage AD. To this end, we assessed the histopathological and AD diagnostic information from the ACT study as well as gene expression data. We tested interaction effects of *GPNMB* gene expression on Aβ and tau by linear regression analyses (Figures 6C and D, Supplementary Tables S7 and S8).

There were significant positive interaction effects of *GPNMB* gene expression on Aβ-tau in the non-dementia group in the HIP and TCx brain regions ($\beta = 0.089$, $p = 0.02$ and $\beta = 0.026$, $p < 0.001$ in HIP and TCx, respectively). Notably, no significant interaction effects were observed at the same sites in the dementia group. These findings suggest that GPNMB+ microglia moderate the Aβ-tau interaction in the early stages of AD.

Discussion

Our results indicated that GPNMB+ microglia moderate the interaction between Aβ and tau in MCI and early AD. We hypothesized that the factors that moderate the Aβ-Tau interaction reside at the intersection of physical and functional interactions between the proteins. To model this, we constructed an integrated functional-physical interaction network in which two different data types, protein co-expression and physical PPIs, were combined into a single network using deep learning-based network integration algorithm. We confirmed that Aβ and tau were present in neighboring modules in the integrated network. Importantly, neither the co-expression information nor physical interaction data alone could capture the Aβ-tau interaction, emphasizing the need to evaluate functional and physical interactions simultaneously. Based on the integrated network, we screened the neighboring proteins for moderating factors and found a stress response module associated with glial cells. The importance of microglia and astrocytes was further supported by histopathological data. We validated these results using snRNA-seq data for human microglia in preclinical and clinical stages.[19,20] We further found that GPNMB+ microglial activation via stress responses marked by *HSPA5* is involved in Aβ-tau interactions. AD clinical cohort data supported the correlation between *GPNMB* protein expression and clinical severity. This finding aligns with those of previous reports indicating that *GPNMB* expression is correlated with disease

pathology.[56] These results suggested that stress response-related modules with *HSPA5* in GPMNB+ activated microglia are drivers of the pathogenesis of AD and function by moderating Aβ-tau interactions in early-stage AD. These factors are potential biomarkers for early-stage AD.

Co-expression network analyses are widely used in AD research.[21–23] However, it is difficult to simultaneously represent physical interactions, such as Aβ-tau interactions or the amyloidome. An approach that integrates networks based on different types of biological information may be effective to explain the complex molecular pathogenesis of AD. In this study, we demonstrated that the integration of physical and functional interaction networks using the BIONIC method[28], a neural network-based algorithm, could capture Aβ-tau interactions and reveal factors that moderate these interactions at cellular resolution.

We identified stress response-related modules in GPNMB+ microglia as moderators of Aβ-tau interactions. The interaction between Aβ and tau has been implicated in the progression of AD, with several factors, such as hypertension,[11] vascular issues,[12] astrocytes,[10] and microglia,[13] highlighted as key mediators or moderators. Our discovery of GPNMB+ microglia as a novel factor aligns with established interactions and provides additional insight by underscoring the role of a specific microglial subtype in moderating Aβ-Tau dynamics. GPNMB+ microglia, a recently identified microglial subtype, are elevated in the frontal white matter and frontal cortex of patients with AD.[57] Additionally, *GPNMB* is expressed in activated microglia.[58] It is associated with AD pathology.[20] Furthermore, the expression of *GNMBP* in microglia is correlated with recently

reported microglial subtypes, such as DAM (disease-associated microglia)[53] and MGnD (microglial neurodegenerative phenotype),[59] which are closely associated with plaques and neurodegeneration.[60] However, their specific functions related to Aβ and tau have not been fully elucidated. Our results provide new insights into the functions of GPNMB+ microglia in the pathogenesis of AD.

Using a pseudo-time analysis of microglial cell populations, we also showed that the *HSPA5* stress response module is synchronized with the activation of GPNMB+ microglia. In other words, the *HSPA5* stress response module may be involved in the Aβ-tau interaction during GPNMB+ microglial activation. It is important to identify the pathways involved in the GPNMB+ microglial activation and the Aβ-tau interaction to validate the role of this cell type in the progression of AD.

A deeper understanding of the mechanisms underlying AD is crucial for the development of effective treatments. Controlling tau phosphorylation, aggregation, and propagation, processes associated with neuronal damage and cognitive decline,[61,62] holds significant promise for mitigating cognitive deterioration in AD. Indeed, the effectiveness of lecanemab, an anti-Aβ antibody, in reducing tau levels in the cerebrospinal fluid and slowing cognitive decline in early-stage AD confirms the presence of Aβ-tau interactions.[9] However, the detailed mechanisms by which the Aβ-tau interaction contributes to AD remain unclear, and studies of the roles of GPNMB+ microglia in these interactions and specifically in the inhibition of their interaction may

provide a basis for developing novel therapeutics that could delay or prevent the progression of AD. This represents a significant shift towards disease-modifying treatments, as current therapies primarily focus on symptom management. Furthermore, the correlations of *GPNMB* expression with CREAD and Braak scores suggest that these factors are biomarkers for the progression of AD. Our data are expected to guide future AD research.

Limitations of the Study

This study had several limitations. First, except for the GPNMB+ microglial data[20], all data were derived from postmortem brains. This raises concerns about the distinction between postmortem effects and AD pathology. Second, in the analyses summarized in Figure 3, protein expression was aggregated by genes, not accounting for multiple isoforms or post-translational modifications, especially in *APP* and *MAPT*. For example, Aβ40 and Aβ42 are produced from *APP* through different processes, and Tau in *MAPT* undergoes various phosphorylation modifications,[63] impacting the disease differently. Histopathological evaluations were used to validate the integrated protein network analysis results. Third, the *GPNMB* gene expression analysis was based on bulk RNA-seq data, which may not specifically reflect GPNMB+ microglia. A detailed analysis of the role of GPNMB+ microglia in AD requires further experimental assays. Nonetheless, our findings contribute new insights into the Aβ-tau interaction and provide directions for the development of AD therapeutics.

Acknowledgments

We extend our thanks to all of the donors who generously contributed invaluable data for this study. We are also grateful to the researchers who made their data publicly available. The results published here are, in whole or in part, based on data obtained from the AD Knowledge Portal (https://adknowledgeportal.org). The study data were provided by the Rush Alzheimer's Disease Center, Rush University Medical Center, Chicago. Data collection was supported through funding by NIA grants P30AG10161 (ROS), R01AG15819 (ROSMAP; genomics and RNAseq), R01AG17917 (MAP), R01AG30146, R01AG36042 (5hC methylation, ATACseq), RC2AG036547 (H3K9Ac), R01AG36836 (RNAseq), R01AG48015 (monocyte RNAseq) RF1AG57473 (single nucleus RNAseq), U01AG32984 (genomic and whole exome sequencing), U01AG46152 (ROSMAP AMP-AD, targeted proteomics), U01AG46161(TMT proteomics), U01AG61356 (whole genome sequencing, targeted proteomics, ROSMAP AMP-AD), the Illinois Department of Public Health (ROSMAP), and the Translational Genomics Research Institute (genomic). Additional phenotypic data were obtained from www.radc.rush.edu. Human AD brain single-nucleus RNA sequencing (snRNA-seq) data were downloaded from the NCBI for Biotechnology Information Gene Expression Omnibus (https://www.ncbi.nlm.nih.gov/geo/). Microglial snRNA-seq data were accessed at https://braincelldat.com/resource and https://doi.org/10.7303/syn2580853. Additionally, the human neuropathological and RNA sequencing datasets used for the linear

regression analysis are available at NIAGADS (https://www.niagads.org/). Figures were created using Bio-Render.com.

Author contributions

Conceptualization and Methodology: M.Y., K.A., Formal Analysis, Investigation, Data Curation, Writing – Original Draft, Visualization: K.A., Resource, Writing – Review & Editing, Supervision, Project Administration and Funding Acquisition: M.Y.

Competing interests

The authors declare no competing interests.

Supplemental information

Document S1. Figures S1–S7

Table S1. Enrichment analysis for each module detected by clustering analysis, related to Figures 1

Table S2. Enrichment analysis for all subnetwork genes, related to Figures 3

Table S3. Enrichment analysis for each community within the subnetwork, related to Figures 3

Table S4. Linear interaction analyses using histopathological data with Tau as the dependent variable, and Aβ, GFAP, and IBA1 as the independent variables, related to Figures 4. For Tau, Tau2 antibody was used.

Table S5. Linear interaction analyses using histopathological data with Tau as the dependent variable, and Aβ, GFAP, and IBA1 as the independent variables, related to Figures 4. For Tau, AT8 antibody was used.

Table S6. Cell composition ratio of microglia subtypes in each pathological condition, related to Figures S6

Table S7. Linear interaction analyses using histopathological data with Tau as the dependent variable, and Aβ and GPNMB gene expression as the independent variables, related to Figures 6. For Tau, Tau2 antibody was used.

Table S8. Linear interaction analyses using histopathological data with Tau as the dependent variable, and Aβ and GPNMB gene expression as the independent variables, related to Figures 6. For Tau, AT8 antibody was used.

Figure legends

Figure 1 Characterization of integrated protein network modules

(A) Schematic representation of the workflow for integrating proteomics and protein–protein interaction (PPI) data and evaluation of integrated features.

(B) Stochastic neighbor embedding (tSNE) plot displaying protein modules.

(C) Upper panels: Uniform Manifold Approximation and Projection (UMAP) visualizations of single-nucleus RNA sequencing (snRNA-seq) data for patients with Alzheimer's disease (AD) (GSE174367)[64] clustered according to cell types (left) and conditions (right) Lower panels: expression levels of proteins within the identified modules.

(D) Representative Gene Ontology (GO) terms enriched in each protein module.

(E) Network depicting the closeness among modules. Closeness was defined by averaging BIONIC-derived features within modules, calculating the Euclidean distances among modules, and taking reciprocals.

Figure 2 Inference of APP-MAPT modulators using a mutual information-based method

(A) Graphical representation of the Modulator Inference by Network Dynamics (MINDy) analysis.

(B) Scatter plot illustrating the relationships between –log10(p-values) and Scores. Points representing p-values less than 0.05 are highlighted in red and are labeled with their

corresponding gene symbols.

Figure 3 Glial cells moderate APP and MAPT interactions

(A) Workflow for network reconstruction from BIONIC analysis results, subnetwork construction using proteins highly associated with intermediary factors, APP and MAPT, and community detection within the network, followed by cell type identification and enrichment analyses for each community.

(B) GO enrichment analysis of the subnetwork, categorized by parent terms using rrvgo[65] software.

(C) Representative GO terms enriched in each community.

(D) Dotplot displaying expression levels of proteins within each community.

Figure 4 Histopathological data analysis validated the roles of microglia and astrocytes as Aβ-tau moderators in early Alzheimer's disease

(A) Schematic of the analytical workflow for linear regression analyses. Samples were sourced from four brain regions: frontal white matter (FWM), hippocampus (HIP), parietal neocortex (PCx), and temporal neocortex (TCx). RNA sequencing and immunohistochemistry data were used.[51] A linear regression was performed, repeated for GFAP and IBA1, and Aβ as predictors of tau interactions.

(B) Significant results of linear regression analyses for each of the four distinct brain regions, with subjects categorized into no dementia and dementia groups.

Figure 5 snRNA-seq Analysis Identifying Enrichment for GPNMB+ Microglia in Community 1

(A, C) Dot plot showing the expression levels of genes aggregated by community in each microglial subtype.[19,20]

(B, D) Min-max normalized combined score for community 1, calculated by multiplying the expression level by the proportion of expressing cells.

Figure 6 GPNMB+ microglia as a possible moderator of the Aβ-tau interaction

(A and B) Heatmaps displaying the correlations between CERAD and Braak scores in samples categorized by the top (A) and bottom (B) 35% of GPNMB expression.

(C) Significant results of linear regression analyses for each of the four distinct brain regions, with subjects categorized into no dementia and dementia groups.

(D) Schematic representation summarizing the findings supporting the roles of both astrocytes and GPNMB+ microglia in the Aβ-tau interaction.

STAR Methods

Key resources table

REAGENT or RESOURCE	SOURCE	IDENTIFIER
Deposited data		
Proteomics data for MCI and early AD cases in the ROSMAP cohort	AD Knowledge Portal	AD Knowledge Portal (https:// adknowledgeportal.synapse.org): https://doi.org/10.7303/syn2580853
AD snRNA-seq dataset	Morabito et al., 2021[64]	GEO: GSE174367
AD microglia dataset	Gazestani et al., 2023[20]	https://braincelldata.org/resource
AD microglia dataset	Sun et al., 2023[19]	https://doi.org/10.7303/syn2580853
Human neuropathological and RNA-seq dataset	Miller JA et al., 2017[51]	https://www.niagads.org/datasets/ng00059
Software and algorithms		
BIONIC v0.2.6	Forster et al., 2022[28]	https://github.com/bowang-lab/BIONIC
R version 4.2.0	R Foundation for Statistical Computing	https://www.r-project.org/
cluster v2.1.4	CRAN	R package (https://cran.r-project.org/web/packages/cluster/index.html)
igraph v1.4.1	CRAN	R package (https://cran.r-project.org/web/packages/igraph/index.html)
Rtsne v.0.16	CRAN	R package (https://cran.r-project.org/web/packages/Rtsne/index.html)
Seurat v.4.3.0	CRAN	R package (https://cran.r-project.org/web/packages/Seurat/readme/README.html)
rrvgo v1.10.0	Bioconductor[65]	R package (https://bioconductor.org/packages/release/bioc/html/rrvgo.html)

clusterProfiler v4.6.2	Bioconductor	R package (https://bioconductor.org/packages/release/bioc/html/clusterProfiler.html)
DOSE v3.24.2	Bioconductor	R package (https://bioconductor.org/packages/release/bioc/html/DOSE.html)

Resource availability

Lead contact

Further information and requests for resources should be directed to and fulfilled by the lead contact, Yusuke Matsui (matsui@met.nagoya-u.ac.jp).

Materials availability

This study did not generate new unique reagents.

Experimental model and subject details

Human subject data

All data analyzed in this study were obtained from publicly available sources.

Method details

Quantification and statistical analysis

Proteomics data from the ROSMAP cohort

For the proteomic analysis, ROSMAP tandem mass tag (TMT) proteomics data were obtained. TMT proteomics is a technique for the simultaneous quantitative analysis of protein expression in multiple samples using LC-MS/MS and is commonly employed in AD research.[22,23,66] The ROSMAP data set included TMT proteomics data for 400 cases with differences in cognitive status (Alzheimer's dementia, other dementia, MCI, or no impairment). Data normalization and

batch correction were conducted according to previous described procedures.[67] Four outlier samples were excluded from subsequent analyses based on a principal component analysis. In this study, ROSMAP TMT data for MCI and early AD cases were included. Early AD was defined according to previously reported criteria: meeting the NIA-AA core clinical criteria for probable AD dementia and having a global CDR score of 0.5 to 1.0 and a CDR memory box score of 0.5 or greater at screening and baseline.[9] Additionally, the MMSE effectively discriminates between CDR stages 0.5, 1, 2, and 3 but performs poorly in the separation of CDR stages zero and 0.5. The previously established MMSE ranges were 30 for no, 26–29 for questionable, 21–25 for mild, 11–20 for moderate, and 0–10 for severe dementia.[68] We defined early AD as having an MMSE score of ≥21.

Proteomics and protein–protein interaction data integration using a Graph Attention Network-based method

To integrate the proteomics and PPI data, total values were calculated for each gene symbol in the proteomics dataset. Pearson correlation coefficients were derived from the proteomics data, retaining only data with Benjamini-Hochberg (BH)-corrected p-values of <0.05. Normalization was performed to set maximum values to 1 and minimum values to 0. For PPI, STRING[31] filtering was used to obtain physical interactions within *Homo sapiens* with confidence scores exceeding 0.7, and normalization was performed to set the maximum values to 1 and minimum values to 0.

Proteomic and PPI data were integrated using a recently reported method, BIONIC,[28] which integrates multiple biological networks while preserving information using graph attention networks.[29] Default values were used for the BIONIC hyperparameters. For both proteomics and PPI data, 4,787 proteins common to both datasets were retained. After integrating the two networks, 512-dimensional features were output for each protein.

Clustering analysis and dimension reduction using features derived from BIONIC

Considering that the data derived from neural networks are nonlinear, clustering was performed following a method similar to that used in snRNA-Seq analyses.[69] After feature calculation using BIONIC and subsequent scaling to Z-scores, Euclidean distances were computed to create a distance matrix. Then, setting k = 25, the k-nearest neighbor method was used to calculate an adjacency matrix and form a graph structure. This graph structure was then subjected to clustering using the Louvain method[70] (resolution = 1) to classify each protein into clusters.

Cluster centroid analysis using BIONIC-derived features

After implementing BIONIC to evaluate the networks derived from proteomic and PPI data, a clustering analysis of proteins was performed. To analyze the relationships between clusters, the average of the feature values for each cluster was calculated as its centroid. Pearson correlation coefficients and Euclidean distances between the clusters were calculated. Furthermore, the

network of clusters was visualized using the reciprocal values of the Euclidean distances as the weights of the edges.

Cell type enrichment analysis based on human brain and microglia snRNA-seq data

For a cell type enrichment analysis, publicly available human brain[64] and microglia[19,20] snRNA-seq data were used. Cell annotations for each dataset were based on publicly available data. The AddModuleScore function was performed using the Seurat package[71] to calculate the average expression levels in each protein community. The combined score was calculated by multiplying the expression level by the proportion of positive cells in each community.

Cell type composition analysis based on human brain and microglia snRNA-seq data

For a cell type composition analysis, publicly available human microglia[20] snRNA-seq data were used. ANOVA was used to compare the frequencies of different microglial subtypes across various conditions (Control, Aβ+, and Aβ+Tau+). Next, for the microglial subtypes "Microglia_GPNMB_LPL" and "Microglia_GPNMB_PLAT," a Tukey HSD test was used to determine specific differences between groups (for cases where ANOVA showed $p < 0.05$).

Gene Ontology functional enrichment analysis

A Gene Ontology (GO) analysis was used to explore the biological functions of our targeted gene

set. The GO biological process (GObp) dataset version 2023.1 was downloaded from the Molecular Signatures Database (MsigDB) (https://www.gsea-msigdb.org/gsea/msigdb). For the analysis, the enrichment function in the clusterProfiler package was used, and values of $p < 0.05$, after Benjamini-Hochberg (BH) correction, were considered significant. rrvgo[65] software was used to summarize the GO terms.

Modulators of the Aβ-tau interaction

To explore Aβ-tau interaction modulators based on proteomics data, a slightly modified version of the MINDy algorithm[34,72] was employed. Briefly, (1) Euclidean distances for APP and MAPT were calculated using BIONIC features, and common elements within the top 5% with respect to proximity were selected for analyses. (2) For each candidate modulator, the top and bottom 35% of proteins with respect to expression levels were segregated and mutual information for APP and Tau was calculated for each group. Mutual information, which measures the interdependence between two random variables X and Y, was defined as follows:

$$MI(X,Y) = \sum x \in X \sum y \in Y\, p(x,y) log(p(x)p(y)p(x,y))$$

Here:

p(x,y) represents the joint probability distribution of *X* and *Y*.

p(x) and *p(y)* are the marginal probability distributions of *X* and *Y*, respectively.

The logarithm base 2 was used.

Subsequently, (3) the difference in mutual information between the top and bottom 35% groups was calculated as follows:

$$\Delta MI = |MI(MAPTMtop35, APPMtop35) - MI(MAPTMbottom35, APPMbottom35)|$$

Here, M_{top35} and $M_{bottom35}$ indicate the APP and MAPT groups in the top 35% and bottom 35% of protein expression levels, respectively. This differentiation is crucial for understanding the difference in mutual information between the two groups, allowing for a clear analysis of the Aβ-Tau interaction modulators. Bootstrapping with 1,000 iterations was then used to compare mutual information, with values of $p < 0.05$ deemed significant.

Next, factors moderating Aβ-Tau interactions were extracted using data obtained from BIONIC and a network analysis was conducted. Among candidate modulators identified in the MINDy analysis, HSPA5, which is closely associated with Aβ[39] and Tau[40], was included in the analysis. The inner product of the BIONIC-derived features was calculated to determine protein similarity, retaining the top 5% for network construction. From this network, the top 5% of factors based on Euclidean distances to *APP*, *MAPT*, and *HSPA5* were retained to form a subnetwork. Community detection within this subnetwork was performed using the leading eigenvector function of the iGraph package[73].

Neuropathological and RNA-seq datasets

The neuropathological and RNA-Seq datasets used in this study were obtained from previously

published works.[51] Neuropathological data include quantitative immunostaining results for the microglial marker IBA1, astrocyte marker GFAP, Aβ, tau, and phosphorylated tau. The datasets included 377 samples collected from the cortical grey (parietal and temporal) and white matter (parietal) as well as the hippocampus. Additionally, the frequency distributions of age, sex, CERAD scores, and Braak scores among the participants were evaluated, differentiating between the no-dementia and dementia groups. Age was compared between the dementia and no dementia groups using a T-test, while sex, Braak score, and CERAD score were compared between the groups using Fisher's exact test.

Linear regression analysis for exploring interaction terms

To explore moderating factors in the Aβ-tau interaction, a linear regression analysis was used to evaluate interaction effects, as described previously.[12] Measurements were performed on formalin-fixed, paraffin-embedded tissue sections (5 μm). For Aβ, the percentage of area covered by Aβ immunoreactivity was used, identifying both Aβ40 and Aβ42. The analysis focused on the percentage of the area covered by Tau2 immunoreactivity, identifying mature neurofibrillary tangles and dystrophic neurites. AT8, an antibody that recognizes phospho-tau (Ser202, Thr205), was also utilized. Interaction effects with Aβ were investigated using immunoreactivities of IBA1 and GFAP and gene expression levels of *GPNMB*. IBA1 was measured as the percentage of area covered by IBA1 immunoreactivity, GFAP as the percentage of area covered by GFAP

immunoreactivity (identifying activated astrocytes), and *GPNMB* gene expression levels were quantified as fragments per kilobase of exon per million reads mapped (FPKM). The interaction effects were evaluated using the *t*-test, with values of $p < 0.05$ considered significant.

Trajectory analysis of human microglia snRNA-seq data

A trajectory analysis was conducted using human microglial snRNA-seq data and the Slingshot package. The default parameters for the slingshot function were utilized, and the getCurves function was used with the following parameters: approx_points = 300, threshold = 0.01, stretch = 0.8, allow.breaks = FALSE, and shrink = 0.99. From the dataset reported by Sun et al. (2023), only microglia were extracted from immune cells for clustering. Clustering was performed using the Seurat package, following the tutorial provided by the Satija Lab (https://satijalab.org/seurat/articles/pbmc3k_tutorial). The settings were FindVariableFeatures with nfeatures = 4000, FindNeighbors, RunUMAP with dims = 1:10, and FindClusters with resolution = 0.5. To visualize gene expression over time, ggplot2 was used and regression curves were generated using generalized additive models (GAM).

Heatmaps of CERAD and Braak scores in the ROSMAP cohort data

To investigate whether GPNMB protein expression moderates the Aβ-tau interaction in patients with MCI and early AD in the ROSMAP cohort, correlations between CERAD and Braak scores

were evaluated. The CERAD score in the ROSMAP cohort is a semiquantitative measure of neuritic plaque density, classified into four scores ranging from 4 to 1, corresponding to no AD, possible AD, probable AD, and definite AD, respectively. The Braak score is a semi-quantitative measure of the severity of neurofibrillary tangle pathology, ranging from 0 to 6, corresponding to Braak stages I–VI. For the top 35% and bottom 35% of patients based on GPNMB protein expression, the frequency of each CERAD and Braak score was visualized using a heatmap.

Data and code availability

All data used in this study are publicly accessible. The proteomic data can be accessed via the AD Knowledge Portal (https://doi.org/10.7303/syn2580853). Human AD brain snRNA-seq and microglia snRNA-seq datasets are available at the NCBI Gene Expression Omnibus (GEO) under accession number GSE174367 and via the following links: https://braincelldat. com/resource and https://doi.org/10.7303/syn2580853. The human neuropathological and RNA sequencing datasets employed for the linear regression analysis can be found at https://www.niagads.org/datasets/ng00059. Additional information required to reanalyze the data reported in this study is available from the lead author upon request.

656

Figure S1 Study Design

A schematic workflow of how the dataset was filtered and utilized in each figure is depicted. Data used for analyses are outlined with black borders, while analyses are framed in blue borders and filled in blue. Specific data applied for sub-objectives are highlighted by black frames within the blue sections. The analysis was conducted in two phases: exploration and validation.

Figure S2. Distances and correlations among protein clusters, related to Figure 2

(A) Heatmap displaying the Euclidean distances between protein communities.

(B) Correlation plot representing the Pearson correlation coefficients among the identified protein communities.

Figure S3. STRING Protein–Protein Interaction (PPI) Networks for MAPT and APP, related to Figure 2

Network diagrams displaying the PPI networks from STRING for (A) MAPT and (B) APP. In both networks, only interactions with a confidence score greater than 0.7, involving physical interactions and experimental validation, were included.

Figure S4 snRNA-seq Analysis Identifying Enrichment for Glial Cell Types in Subnetwork Communities, related to Figure 3

The min-max-normalized combined score for each community was calculated by multiplying the expression level by the proportion of expressing cells, based on the same dataset as in Figure 3[64] (A) and a validation cohort[19,20] (B), (C).

Figure S5 Characteristics of the ACT study Participants, related to Figure 4

The distribution of age (A), sex (B), CERAD score (C), and Braak score (D) of the ACT study participants differentiated between the no-dementia and dementia groups.

Figure S6 Cell Type Analysis for Control, Aβ+, and Aβ+Tau+ groups, Related to Figure 5

Cell type compositions were compared among Control, Aβ+, and Aβ+Tau+ groups. Box plots displaying the distribution of cell type frequencies for each patient group. Results were analyzed using ANOVA, followed by Tukey's post-hoc test for pairwise comparisons when significant ANOVA results were observed.

Figure S7 Trajectory Analysis and pseudotime gene expression of candidate Aβ-tau-moderating factors, Related to Figure 5

(A), (D) Slingshot trajectory inference applied to microglia revealed three lineages.

(B), (E) Pseudotime gene expression analysis of modulator candidate genes predicted using MINDy and GPNMB in a lineage. Gene expression levels are shown for the lineages that are highlighted in bold in (A) and (D), respectively.

References

1. d'Errico, P., and Meyer-Luehmann, M. (2020). Mechanisms of Pathogenic Tau and Aβ Protein Spreading in Alzheimer's Disease. Front. Aging Neurosci. *12*, 265.

2. Knopman, D.S., Amieva, H., Petersen, R.C., Chételat, G., Holtzman, D.M., Hyman, B.T., Nixon, R.A., and Jones, D.T. (2021). Alzheimer disease. Nature Reviews Disease Primers *7*, 1–21.

3. Congdon, E.E., Ji, C., Tetlow, A.M., Jiang, Y., and Sigurdsson, E.M. (2023). Tau-targeting therapies for Alzheimer disease: current status and future directions. Nat. Rev. Neurol. *19*, 715–736.

4. Bloom, G.S. (2014). Amyloid-β and tau: the trigger and bullet in Alzheimer disease pathogenesis. JAMA Neurol. *71*, 505–508.

5. Busche, M.A., and Hyman, B.T. (2020). Synergy between amyloid-β and tau in Alzheimer's disease. Nat. Neurosci. *23*, 1183–1193.

6. Zhang, H., Wei, W., Zhao, M., Ma, L., Jiang, X., Pei, H., Cao, Y., and Li, H. (2021). Interaction between Aβ and Tau in the Pathogenesis of Alzheimer's Disease. Int. J. Biol. Sci. *17*, 2181–2192.

7. Lee, W.J., Brown, J.A., Kim, H.R., La Joie, R., Cho, H., Lyoo, C.H., Rabinovici, G.D., Seong,

J.-K., Seeley, W.W., and Alzheimer's Disease Neuroimaging Initiative (2022). Regional Aβ-tau interactions promote onset and acceleration of Alzheimer's disease tau spreading. Neuron *110*, 1932-1943.e5.

8. Aksman, L.M., Oxtoby, N.P., Scelsi, M.A., Wijeratne, P.A., Young, A.L., Alves, I.L., Collij, L.E., Vogel, J.W., Barkhof, F., Alexander, D.C., et al. (2023). A data-driven study of Alzheimer's disease related amyloid and tau pathology progression. Brain *146*, 4935–4948.

9. van Dyck, C.H., Swanson, C.J., Aisen, P., Bateman, R.J., Chen, C., Gee, M., Kanekiyo, M., Li, D., Reyderman, L., Cohen, S., et al. (2023). Lecanemab in Early Alzheimer's Disease. N. Engl. J. Med. *388*, 9–21.

10. Bellaver, B., Povala, G., Ferreira, P.C.L., Ferrari-Souza, J.P., Leffa, D.T., Lussier, F.Z., Benedet, A.L., Ashton, N.J., Triana-Baltzer, G., Kolb, H.C., et al. (2023). Astrocyte reactivity influences amyloid-β effects on tau pathology in preclinical Alzheimer's disease. Nat. Med. *29*, 1775–1781.

11. Kim, T., Yi, D., Byun, M.S., Ahn, H., Jung, J.H., Kong, N., Kim, M.J., Jung, G., Lee, J.-Y., Lee, Y.-S., et al. (2022). Synergistic interaction of high blood pressure and cerebral beta-amyloid on tau pathology. Alzheimers. Res. Ther. *14*, 193.

12. Coomans, E.M., van Westen, D., Pichet Binette, A., Strandberg, O., Spotorno, N., Serrano, G.E., Beach, T.G., Palmqvist, S., Stomrud, E., Ossenkoppele, R., et al. (2023). Interactions

between vascular burden and amyloid-β pathology on trajectories of tau accumulation. Brain. 10.1093/brain/awad317.

13. Yang, H.-S., Teng, L., Kang, D., Menon, V., Ge, T., Finucane, H.K., Schultz, A.P., Properzi, M., Klein, H.-U., Chibnik, L.B., et al. (2023). Cell-type-specific Alzheimer's disease polygenic risk scores are associated with distinct disease processes in Alzheimer's disease. Nat. Commun. *14*, 1–13.

14. Mathys, H., Peng, Z., Boix, C.A., Victor, M.B., Leary, N., Babu, S., Abdelhady, G., Jiang, X., Ng, A.P., Ghafari, K., et al. (2023). Single-cell atlas reveals correlates of high cognitive function, dementia, and resilience to Alzheimer's disease pathology. Cell *186*, 4365-4385.e27.

15. Zhou, Y., Song, W.M., Andhey, P.S., Swain, A., Levy, T., Miller, K.R., Poliani, P.L., Cominelli, M., Grover, S., Gilfillan, S., et al. (2020). Human and mouse single-nucleus transcriptomics reveal TREM2-dependent and TREM2-independent cellular responses in Alzheimer's disease. Nat. Med. *26*, 131–142.

16. Olah, M., Menon, V., Habib, N., Taga, M.F., Ma, Y., Yung, C.J., Cimpean, M., Khairallah, A., Coronas-Samano, G., Sankowski, R., et al. (2020). Single cell RNA sequencing of human microglia uncovers a subset associated with Alzheimer's disease. Nat. Commun. *11*, 6129.

17. Grubman, A., Chew, G., Ouyang, J.F., Sun, G., Choo, X.Y., McLean, C., Simmons, R.K.,

Buckberry, S., Vargas-Landin, D.B., Poppe, D., et al. (2019). A single-cell atlas of entorhinal cortex from individuals with Alzheimer's disease reveals cell-type-specific gene expression regulation. Nat. Neurosci. *22*, 2087–2097.

18. Mathys, H., Davila-Velderrain, J., Peng, Z., Gao, F., Mohammadi, S., Young, J.Z., Menon, M., He, L., Abdurrob, F., Jiang, X., et al. (2019). Single-cell transcriptomic analysis of Alzheimer's disease. Nature *570*, 332–337.

19. Sun, N., Victor, M.B., Park, Y.P., Xiong, X., Scannail, A.N., Leary, N., Prosper, S., Viswanathan, S., Luna, X., Boix, C.A., et al. (2023). Human microglial state dynamics in Alzheimer's disease progression. Cell *186*, 4386-4403.e29.

20. Gazestani, V., Kamath, T., Nadaf, N.M., Dougalis, A., Burris, S.J., Rooney, B., Junkkari, A., Vanderburg, C., Pelkonen, A., Gomez-Budia, M., et al. (2023). Early Alzheimer's disease pathology in human cortex involves transient cell states. Cell *186*, 4438-4453.e23.

21. Neff, R.A., Wang, M., Vatansever, S., Guo, L., Ming, C., Wang, Q., Wang, E., Horgusluoglu-Moloch, E., Song, W.-M., Li, A., et al. (2021). Molecular subtyping of Alzheimer's disease using RNA sequencing data reveals novel mechanisms and targets. Science Advances *7*, eabb5398.

22. Johnson, E.C.B., Carter, E.K., Dammer, E.B., Duong, D.M., Gerasimov, E.S., Liu, Y., Liu, J., Betarbet, R., Ping, L., Yin, L., et al. (2022). Large-scale deep multi-layer analysis of

Alzheimer's disease brain reveals strong proteomic disease-related changes not observed at the RNA level. Nat. Neurosci. *25*, 213–225.

23. Bai, B., Wang, X., Li, Y., Chen, P.-C., Yu, K., Dey, K.K., Yarbro, J.M., Han, X., Lutz, B.M., Rao, S., et al. (2020). Deep Multilayer Brain Proteomics Identifies Molecular Networks in Alzheimer's Disease Progression. Neuron *105*, 975-991.e7.

24. Cho, H., Berger, B., and Peng, J. (2016). Compact Integration of Multi-Network Topology for Functional Analysis of Genes. Cell Syst *3*, 540-548.e5.

25. Chen, G., and Liu, Z.-P. (2022). Graph attention network for link prediction of gene regulations from single-cell RNA-sequencing data. Bioinformatics *38*, 4522–4529.

26. Schulte-Sasse, R., Budach, S., Hnisz, D., and Marsico, A. (2021). Integration of multiomics data with graph convolutional networks to identify new cancer genes and their associated molecular mechanisms. Nature Machine Intelligence *3*, 513–526.

27. Peng, W., Tang, Q., Dai, W., and Chen, T. (2022). Improving cancer driver gene identification using multi-task learning on graph convolutional network. Brief. Bioinform. *23*. 10.1093/bib/bbab432.

28. Forster, D.T., Li, S.C., Yashiroda, Y., Yoshimura, M., Li, Z., Isuhuaylas, L.A.V., Itto-Nakama, K., Yamanaka, D., Ohya, Y., Osada, H., et al. (2022). BIONIC: biological network integration

using convolutions. Nat. Methods *19*, 1250–1261.

29. Veličković, P., Cucurull, G., Casanova, A., Romero, A., Liò, P., and Bengio, Y. (2017). Graph Attention Networks. arXiv [stat.ML].

30. Li, P., Jiang, Z., Liu, T., Liu, X., Qiao, H., and Yao, X. (2024). Improving drug response prediction via integrating gene relationships with deep learning. Brief. Bioinform. *25*. 10.1093/bib/bbae153.

31. Szklarczyk, D., Gable, A.L., Lyon, D., Junge, A., Wyder, S., Huerta-Cepas, J., Simonovic, M., Doncheva, N.T., Morris, J.H., Bork, P., et al. (2019). STRING v11: protein-protein association networks with increased coverage, supporting functional discovery in genome-wide experimental datasets. Nucleic Acids Res. *47*, D607–D613.

32. Young, C.B., Johns, E., Kennedy, G., Belloy, M.E., Insel, P.S., Greicius, M.D., Sperling, R.A., Johnson, K.A., Poston, K.L., Mormino, E.C., et al. (2023). APOE effects on regional tau in preclinical Alzheimer's disease. Mol. Neurodegener. *18*, 1.

33. Verghese, P.B., Castellano, J.M., Garai, K., Wang, Y., Jiang, H., Shah, A., Bu, G., Frieden, C., and Holtzman, D.M. (2013). ApoE influences amyloid-β (Aβ) clearance despite minimal apoE/Aβ association in physiological conditions. Proc. Natl. Acad. Sci. U. S. A. *110*, E1807-16.

34. Wang, K., Saito, M., Bisikirska, B.C., Alvarez, M.J., Lim, W.K., Rajbhandari, P., Shen, Q., Nemenman, I., Basso, K., Margolin, A.A., et al. (2009). Genome-wide identification of post-translational modulators of transcription factor activity in human B cells. Nat. Biotechnol. *27*, 829–839.

35. Stetler, R.A., Gan, Y., Zhang, W., Liou, A.K., Gao, Y., Cao, G., and Chen, J. (2010). Heat shock proteins: cellular and molecular mechanisms in the central nervous system. Prog. Neurobiol. *92*, 184–211.

36. Das, S., Ramakrishna, S., and Kim, K.-S. (2020). Critical Roles of Deubiquitinating Enzymes in the Nervous System and Neurodegenerative Disorders. Mol. Cells *43*, 203–214.

37. Genau, H.M., Huber, J., Baschieri, F., Akutsu, M., Dötsch, V., Farhan, H., Rogov, V., and Behrends, C. (2015). CUL3-KBTBD6/KBTBD7 ubiquitin ligase cooperates with GABARAP proteins to spatially restrict TIAM1-RAC1 signaling. Mol. Cell *57*, 995–1010.

38. Ichijo, H., Nishida, E., Irie, K., ten Dijke, P., Saitoh, M., Moriguchi, T., Takagi, M., Matsumoto, K., Miyazono, K., and Gotoh, Y. (1997). Induction of apoptosis by ASK1, a mammalian MAPKKK that activates SAPK/JNK and p38 signaling pathways. Science *275*, 90–94.

39. Andrew, R.J., Fisher, K., Heesom, K.J., Kellett, K.A.B., and Hooper, N.M. (2019). Quantitative interaction proteomics reveals differences in the interactomes of amyloid precursor protein isoforms. J. Neurochem. *149*, 399–412.

40. Drummond, E., Pires, G., MacMurray, C., Askenazi, M., Nayak, S., Bourdon, M., Safar, J., Ueberheide, B., and Wisniewski, T. (2020). Phosphorylated tau interactome in the human Alzheimer's disease brain. Brain *143*, 2803–2817.

41. Ajoolabady, A., Lindholm, D., Ren, J., and Pratico, D. (2022). ER stress and UPR in Alzheimer's disease: mechanisms, pathogenesis, treatments. Cell Death Dis. *13*, 1–15.

42. Gorbatyuk, M.S., and Gorbatyuk, O.S. (2013). The Molecular Chaperone GRP78/BiP as a Therapeutic Target for Neurodegenerative Disorders: A Mini Review. J. Genet. Syndr. Gene Ther. *4*. 10.4172/2157-7412.1000128.

43. Yang, Y., Turner, R.S., and Gaut, J.R. (1998). The chaperone BiP/GRP78 binds to amyloid precursor protein and decreases Abeta40 and Abeta42 secretion. J. Biol. Chem. *273*, 25552–25555.

44. Hoshino, T., Nakaya, T., Araki, W., Suzuki, K., Suzuki, T., and Mizushima, T. (2007). Endoplasmic reticulum chaperones inhibit the production of amyloid-beta peptides. Biochem. J *402*, 581–589.

45. Sakono, M., and Kidani, T. (2017). ATP-independent inhibition of amyloid beta fibrillation by the endoplasmic reticulum resident molecular chaperone GRP78. Biochem. Biophys. Res. Commun. *493*, 500–503.

46. Fontaine, S.N., Rauch, J.N., Nordhues, B.A., Assimon, V.A., Stothert, A.R., Jinwal, U.K., Sabbagh, J.J., Chang, L., Stevens, S.M., Jr, Zuiderweg, E.R.P., et al. (2015). Isoform-selective Genetic Inhibition of Constitutive Cytosolic Hsp70 Activity Promotes Client Tau Degradation Using an Altered Co-chaperone Complement. J. Biol. Chem. *290*, 13115–13127.

47. Moll, A., Ramirez, L.M., Ninov, M., Schwarz, J., Urlaub, H., and Zweckstetter, M. (2022). Hsp multichaperone complex buffers pathologically modified Tau. Nat. Commun. *13*, 1–13.

48. Shao, Y., Xu, Y., Di, H., Shi, X., Wang, Y., Liu, H., and Song, L. (2023). The inhibition of ORMDL3 prevents Alzheimer's disease through ferroptosis by PERK/ATF4/HSPA5 pathway. IET Nanobiotechnol. *17*, 182–196.

49. Gao, H., Lei, X., Ye, S., Ye, T., Hua, R., Wang, G., Song, H., Zhou, P., Wang, Y., and Cai, B. (2022). Genistein attenuates memory impairment in Alzheimer's disease via ERS-mediated apoptotic pathway in vivo and in vitro. J. Nutr. Biochem. *109*, 109118.

50. Castanho, I., Murray, T.K., Hannon, E., Jeffries, A., Walker, E., Laing, E., Baulf, H., Harvey, J., Bradshaw, L., Randall, A., et al. (2020). Transcriptional Signatures of Tau and Amyloid Neuropathology. Cell Rep. *30*, 2040-2054.e5.

51. Miller, J.A., Guillozet-Bongaarts, A., Gibbons, L.E., Postupna, N., Renz, A., Beller, A.E., Sunkin, S.M., Ng, L., Rose, S.E., Smith, K.A., et al. (2017). Neuropathological and

transcriptomic characteristics of the aged brain. Elife *6*. 10.7554/eLife.31126.

52. Braak, H., and Braak, E. (1991). Neuropathological stageing of Alzheimer-related changes. Acta Neuropathol. *82*, 239–259.

53. Keren-Shaul, H., Spinrad, A., Weiner, A., Matcovitch-Natan, O., Dvir-Szternfeld, R., Ulland, T.K., David, E., Baruch, K., Lara-Astaiso, D., Toth, B., et al. (2017). A Unique Microglia Type Associated with Restricting Development of Alzheimer's Disease. Cell *169*, 1276-1290.e17.

54. Noda, Y., Tsuruma, K., Takata, M., Ishisaka, M., Tanaka, H., Nakano, Y., Nagahara, Y., Shimazawa, M., and Hara, H. (2017). GPNMB Induces BiP Expression by Enhancing Splicing of BiP Pre-mRNA during the Endoplasmic Reticulum Stress Response. Sci. Rep. *7*, 12160.

55. Street, K., Risso, D., Fletcher, R.B., Das, D., Ngai, J., Yosef, N., Purdom, E., and Dudoit, S. (2018). Slingshot: cell lineage and pseudotime inference for single-cell transcriptomics. BMC Genomics *19*, 477.

56. Doroszkiewicz, J., Kulczynska-Przybik, A., Dulewicz, M., Borawska, R., Slowik, A., and Mroczko, B. (2023). The cerebrospinal fluid Glycoprotein Nonmetastatic Melanoma Protein B (GPNMB) concentration in Alzheimer's Disease (AD). Alzheimers. Dement. *19*. 10.1002/alz.062120.

57. Satoh, J.-I., Kino, Y., Yanaizu, M., Ishida, T., and Saito, Y. (2019). Microglia express GPNMB in the brains of Alzheimer's disease and Nasu-Hakola disease. Intractable Rare Dis Res *8*, 120–128.

58. Hüttenrauch, M., Ogorek, I., Klafki, H., Otto, M., Stadelmann, C., Weggen, S., Wiltfang, J., and Wirths, O. (2018). Glycoprotein NMB: a novel Alzheimer's disease associated marker expressed in a subset of activated microglia. Acta Neuropathol Commun *6*, 108.

59. Krasemann, S., Madore, C., Cialic, R., Baufeld, C., Calcagno, N., El Fatimy, R., Beckers, L., O'Loughlin, E., Xu, Y., Fanek, Z., et al. (2017). The TREM2-APOE Pathway Drives the Transcriptional Phenotype of Dysfunctional Microglia in Neurodegenerative Diseases. Immunity *47*, 566-581.e9.

60. Sobue, A., Komine, O., and Yamanaka, K. (2023). Neuroinflammation in Alzheimer's disease: microglial signature and their relevance to disease. Inflamm. Regen. *43*, 26.

61. Iqbal, K., Alonso, A. del C., Chen, S., Chohan, M.O., El-Akkad, E., Gong, C.-X., Khatoon, S., Li, B., Liu, F., Rahman, A., et al. (2005). Tau pathology in Alzheimer disease and other tauopathies. Biochim. Biophys. Acta *1739*, 198–210.

62. Bejanin, A., Schonhaut, D.R., La Joie, R., Kramer, J.H., Baker, S.L., Sosa, N., Ayakta, N., Cantwell, A., Janabi, M., Lauriola, M., et al. (2017). Tau pathology and neurodegeneration contribute to cognitive impairment in Alzheimer's disease. Brain *140*, 3286–3300.

63. Wegmann, S., Biernat, J., and Mandelkow, E. (2021). A current view on Tau protein phosphorylation in Alzheimer's disease. Curr. Opin. Neurobiol. *69*, 131–138.

64. Morabito, S., Miyoshi, E., Michael, N., Shahin, S., Martini, A.C., Head, E., Silva, J., Leavy, K., Perez-Rosendahl, M., and Swarup, V. (2021). Single-nucleus chromatin accessibility and transcriptomic characterization of Alzheimer's disease. Nat. Genet. *53*, 1143–1155.

65. Sayols, S. (2023). rrvgo: a Bioconductor package for interpreting lists of Gene Ontology terms. MicroPubl Biol *2023*. 10.17912/micropub.biology.000811.

66. Johnson, E.C.B., Dammer, E.B., Duong, D.M., Ping, L., Zhou, M., Yin, L., Higginbotham, L.A., Guajardo, A., White, B., Troncoso, J.C., et al. (2020). Large-scale proteomic analysis of Alzheimer's disease brain and cerebrospinal fluid reveals early changes in energy metabolism associated with microglia and astrocyte activation. Nat. Med. *26*, 769–780.

67. ROSMAP_ProteomicsTMT_BatchCorrectionOC.pdf. Preprint.

68. Perneczky, R., Wagenpfeil, S., Komossa, K., Grimmer, T., Diehl, J., and Kurz, A. (2006). Mapping scores onto stages: mini-mental state examination and clinical dementia rating. Am. J. Geriatr. Psychiatry *14*, 139–144.

69. Macosko, E.Z., Basu, A., Satija, R., Nemesh, J., Shekhar, K., Goldman, M., Tirosh, I., Bialas, A.R., Kamitaki, N., Martersteck, E.M., et al. (2015). Highly Parallel Genome-wide Expression

Profiling of Individual Cells Using Nanoliter Droplets. Cell *161*, 1202–1214.

70. Blondel, V.D., Guillaume, J.-L., Lambiotte, R., and Lefebvre, E. (2008). Fast unfolding of communities in large networks. J. Stat. Mech. *2008*, P10008.

71. Hao, Y., Hao, S., Andersen-Nissen, E., Mauck, W.M., 3rd, Zheng, S., Butler, A., Lee, M.J., Wilk, A.J., Darby, C., Zager, M., et al. (2021). Integrated analysis of multimodal single-cell data. Cell *184*, 3573-3587.e29.

72. Campbell, T.M., Castro, M.A.A., Ponder, B.A.J., and Meyer, K.B. (2016). Identification of Post-Transcriptional Modulators of Breast Cancer Transcription Factor Activity Using MINDy. PLoS One *11*, e0168770.

73. Csárdi, G., and Nepusz, T. (2006). The igraph software package for complex network research. https://www.semanticscholar.org › ...https://www.semanticscholar.org › ...

Graphical Abstract

Protein Expression and Protein-Protein Interaction Network Integration

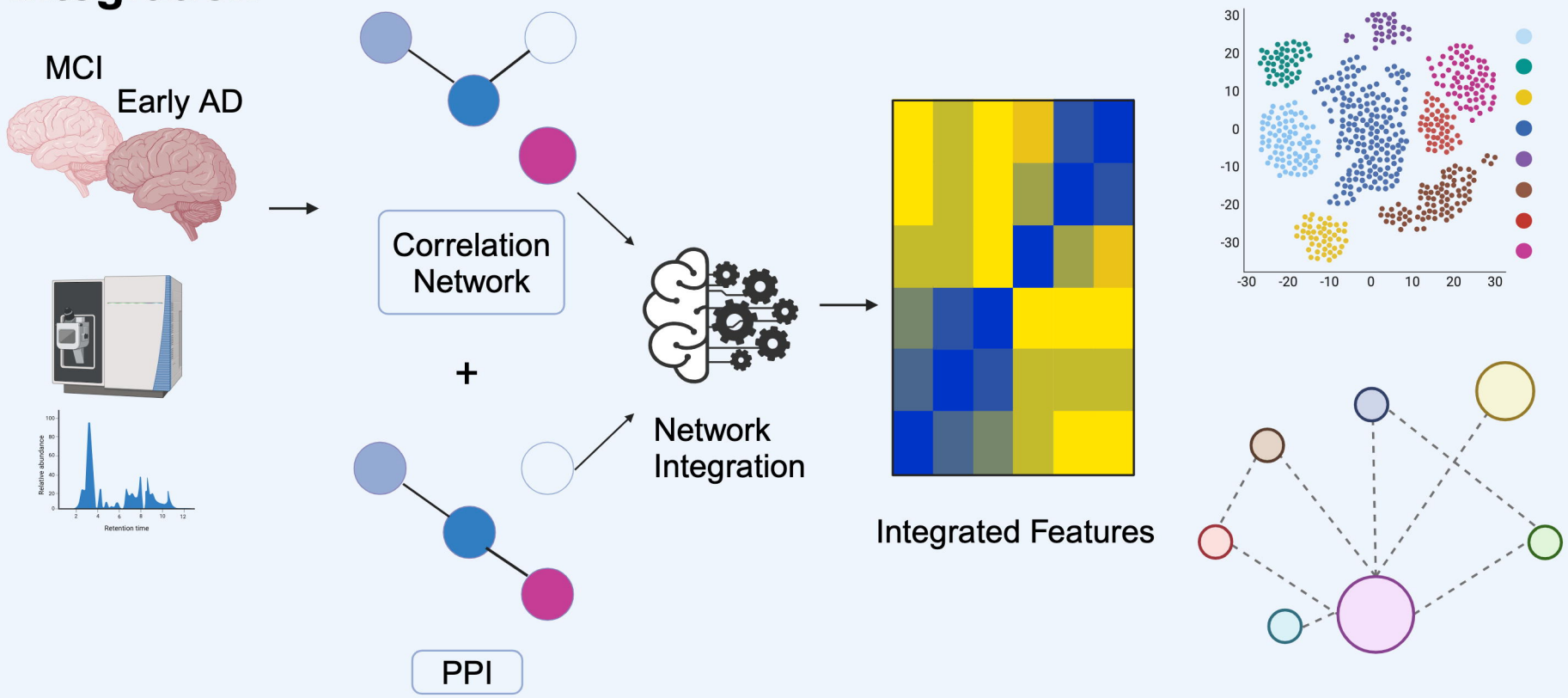

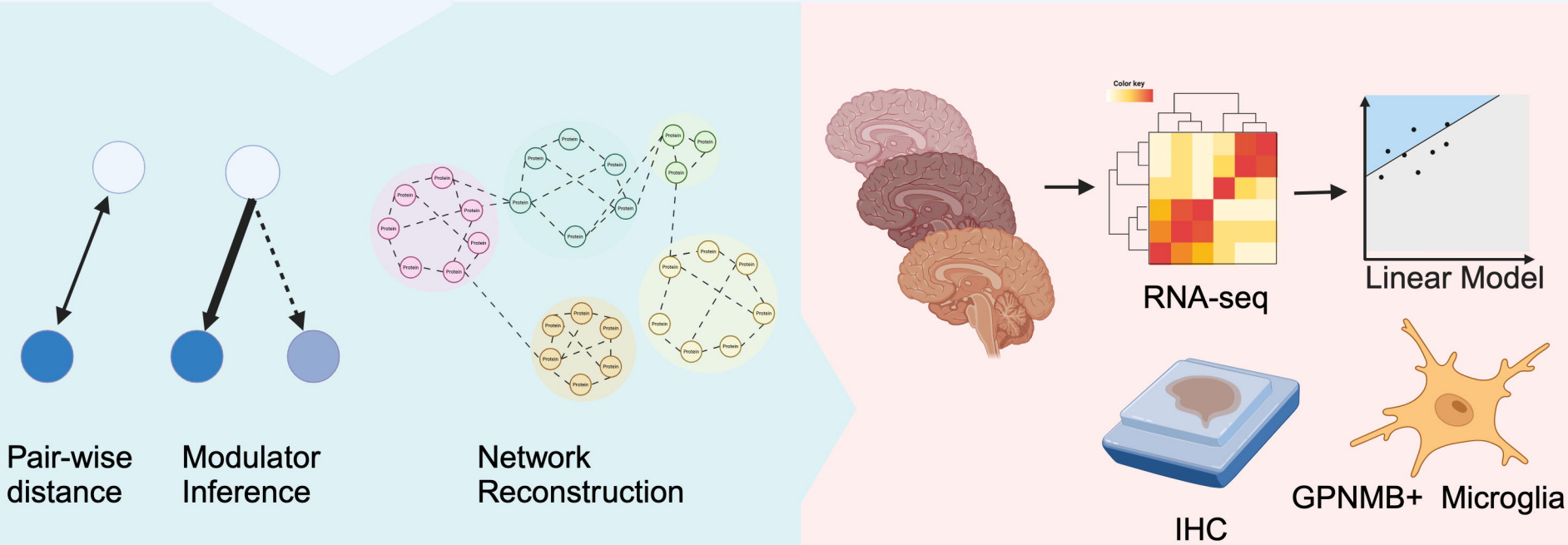

Exploration of Aβ-Tau Interaction Mediating Factor

Validation of Mediating Factor and Cell Subtype Analysis

Fig.1

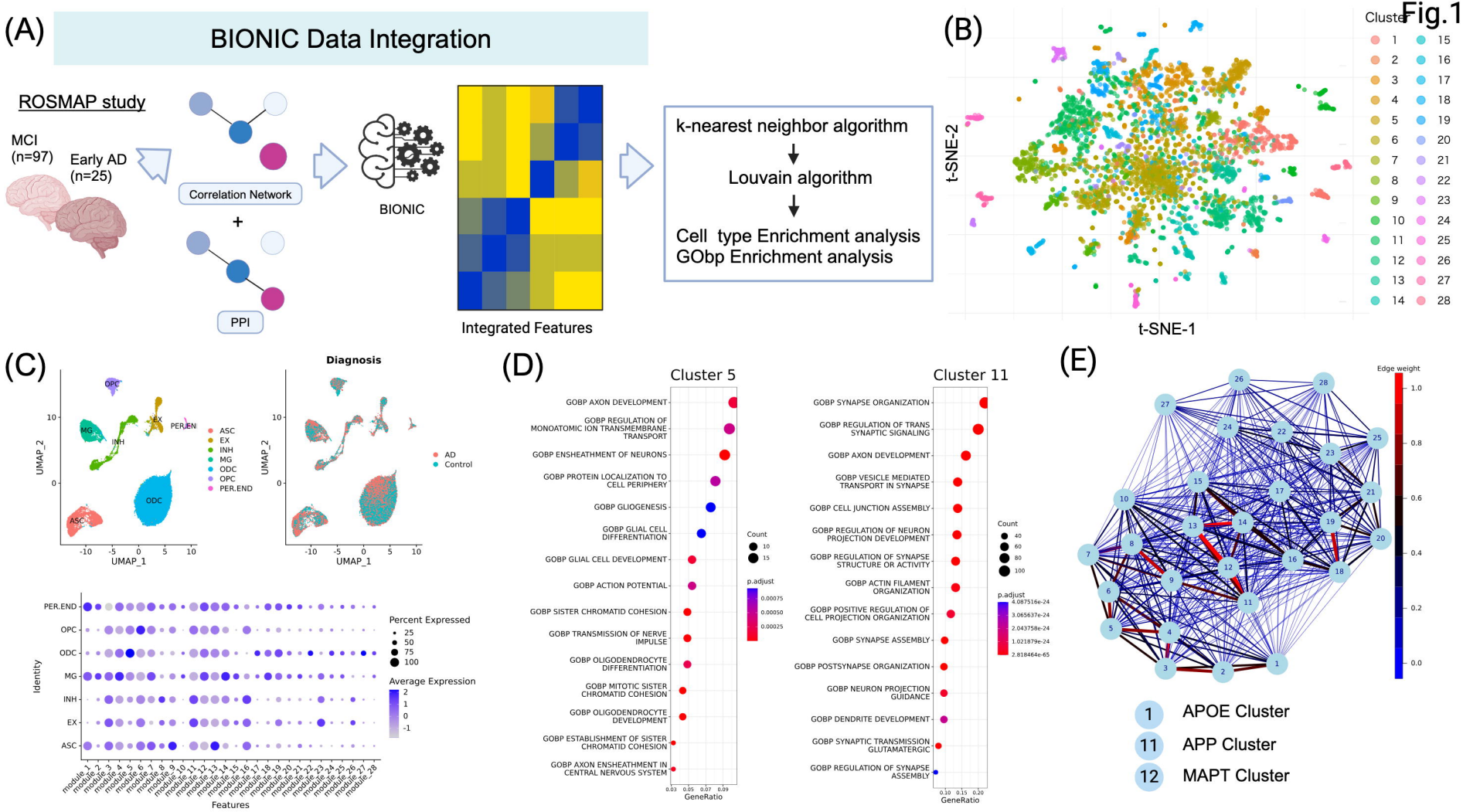
(A)
BIONIC Data Integration
ROSMAP study
MCI (n=97)
Early AD (n=25)
Correlation Network
+
PPI
BIONIC
Integrated Features
k-nearest neighbor algorithm
Louvain algorithm
Cell type Enrichment analysis
GObp Enrichment analysis
(B)
Cluster
t-SNE-2
t-SNE-1
(C)
Diagnosis
UMAP_1
UMAP_2
ASC
EX
INH
MG
ODC
OPC
PER.END
AD
Control
Percent Expressed
Average Expression
Identity
Features
(D)
Cluster 5
GOBP AXON DEVELOPMENT
GOBP REGULATION OF MONOATOMIC ION TRANSMEMBRANE TRANSPORT
GOBP ENSHEATHMENT OF NEURONS
GOBP PROTEIN LOCALIZATION TO CELL PERIPHERY
GOBP GLIOGENESIS
GOBP GLIAL CELL DIFFERENTIATION
GOBP GLIAL CELL DEVELOPMENT
GOBP ACTION POTENTIAL
GOBP SISTER CHROMATID COHESION
GOBP TRANSMISSION OF NERVE IMPULSE
GOBP OLIGODENDROCYTE DIFFERENTIATION
GOBP MITOTIC SISTER CHROMATID COHESION
GOBP OLIGODENDROCYTE DEVELOPMENT
GOBP ESTABLISHMENT OF SISTER CHROMATID COHESION
GOBP AXON ENSHEATHMENT IN CENTRAL NERVOUS SYSTEM
Count
p.adjust
GeneRatio
Cluster 11
GOBP SYNAPSE ORGANIZATION
GOBP REGULATION OF TRANS SYNAPTIC SIGNALING
GOBP AXON DEVELOPMENT
GOBP VESICLE MEDIATED TRANSPORT IN SYNAPSE
GOBP CELL JUNCTION ASSEMBLY
GOBP REGULATION OF NEURON PROJECTION DEVELOPMENT
GOBP REGULATION OF SYNAPSE STRUCTURE OR ACTIVITY
GOBP ACTIN FILAMENT ORGANIZATION
GOBP POSITIVE REGULATION OF CELL PROJECTION ORGANIZATION
GOBP SYNAPSE ASSEMBLY
GOBP POSTSYNAPSE ORGANIZATION
GOBP NEURON PROJECTION GUIDANCE
GOBP DENDRITE DEVELOPMENT
GOBP SYNAPTIC TRANSMISSION GLUTAMATERGIC
GOBP REGULATION OF SYNAPSE ASSEMBLY
(E)
Edge weight
1 APOE Cluster
11 APP Cluster
12 MAPT Cluster

Fig.2

(A)

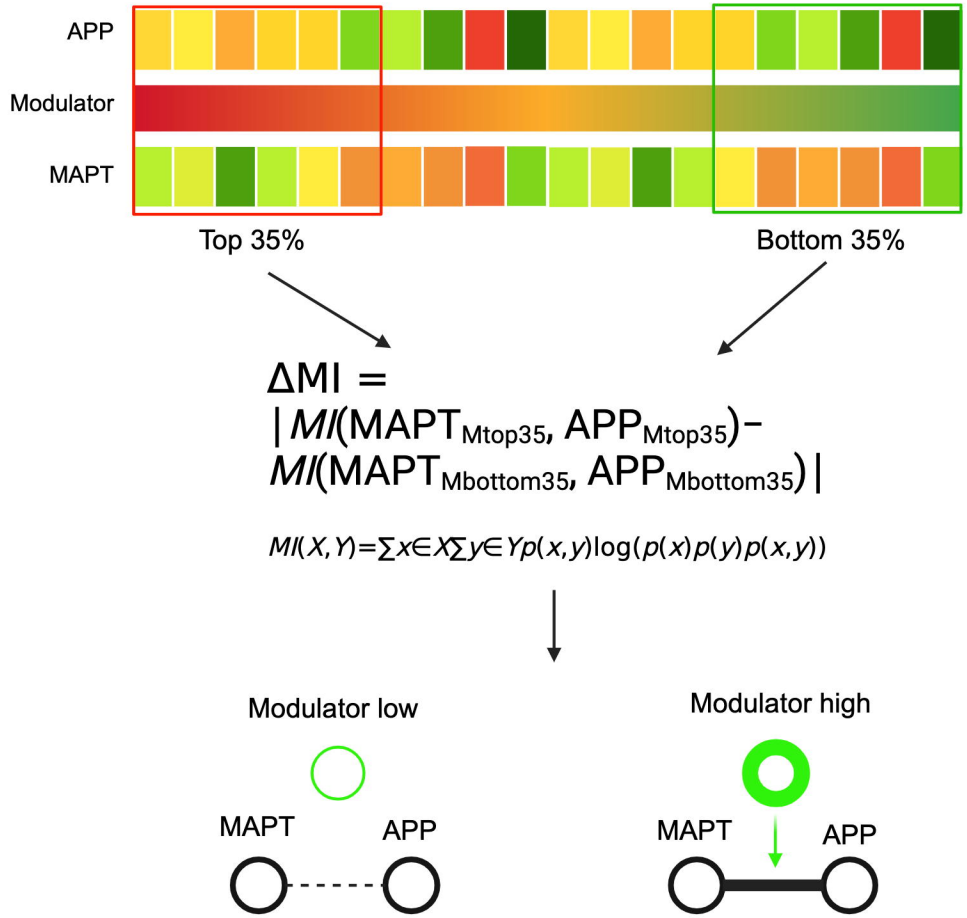
APP
Modulator
MAPT
Top 35%
Bottom 35%
ΔMI =
|MI(MAPT_Mtop35, APP_Mtop35)−
MI(MAPT_Mbottom35, APP_Mbottom35)|
MI(X,Y)=∑x∈X∑y∈Yp(x,y)log(p(x)p(y)p(x,y))
Modulator low
MAPT
APP
Modulator high
MAPT
APP

(B)

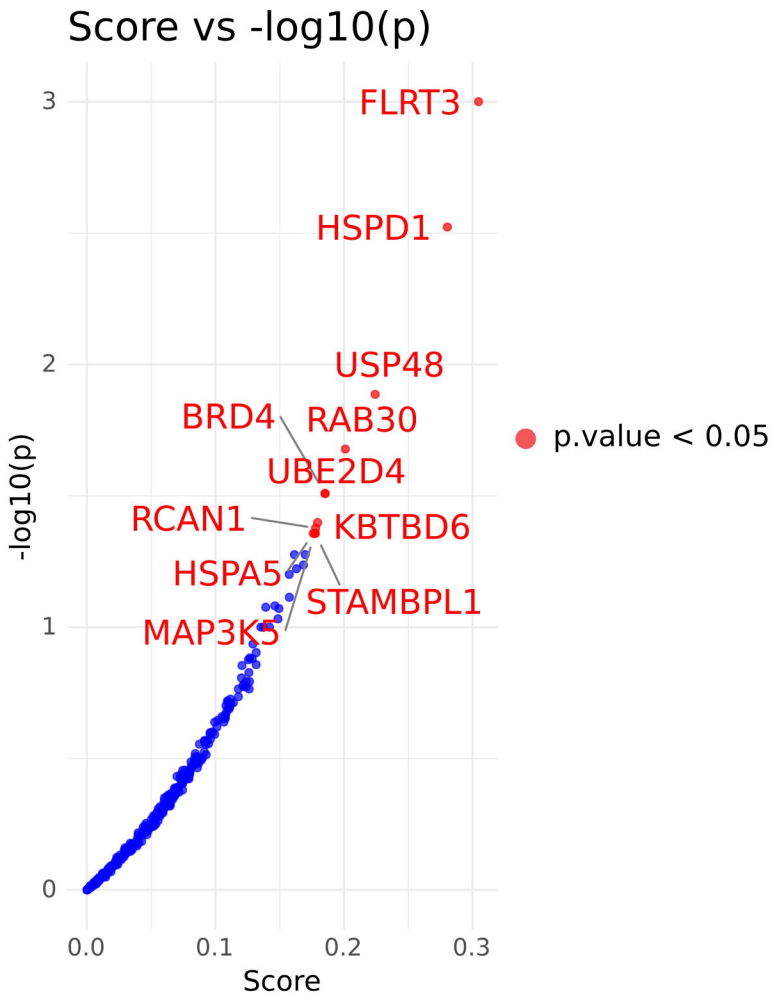
Score vs -log10(p)
FLRT3
HSPD1
USP48
BRD4
RAB30
UBE2D4
RCAN1
KBTBD6
HSPA5
STAMBPL1
MAP3K5
p.value < 0.05
-log10(p)
Score
0
1
2
3
0.0
0.1
0.2
0.3

Fig.3

(A)

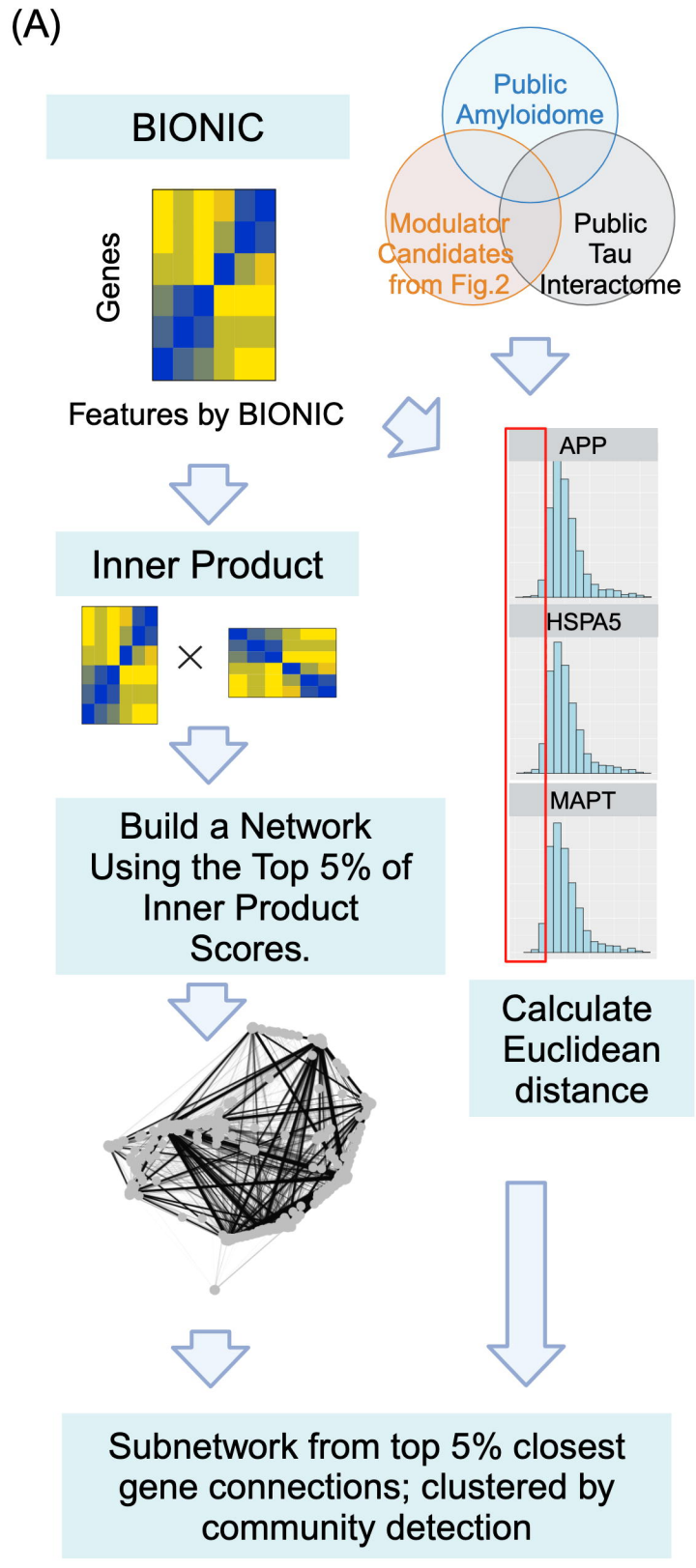

Cell type	Mechanism	
Oligodendrocyte	Neuron death, Stress response	APP
Neuron, Microglia	Kinase activity	MAPT, HSPA5
Microglia	Migration, Chemotaxis	
OPC, Astrocyte, Microglia	Neuron death, Kinase activity	GPNMB

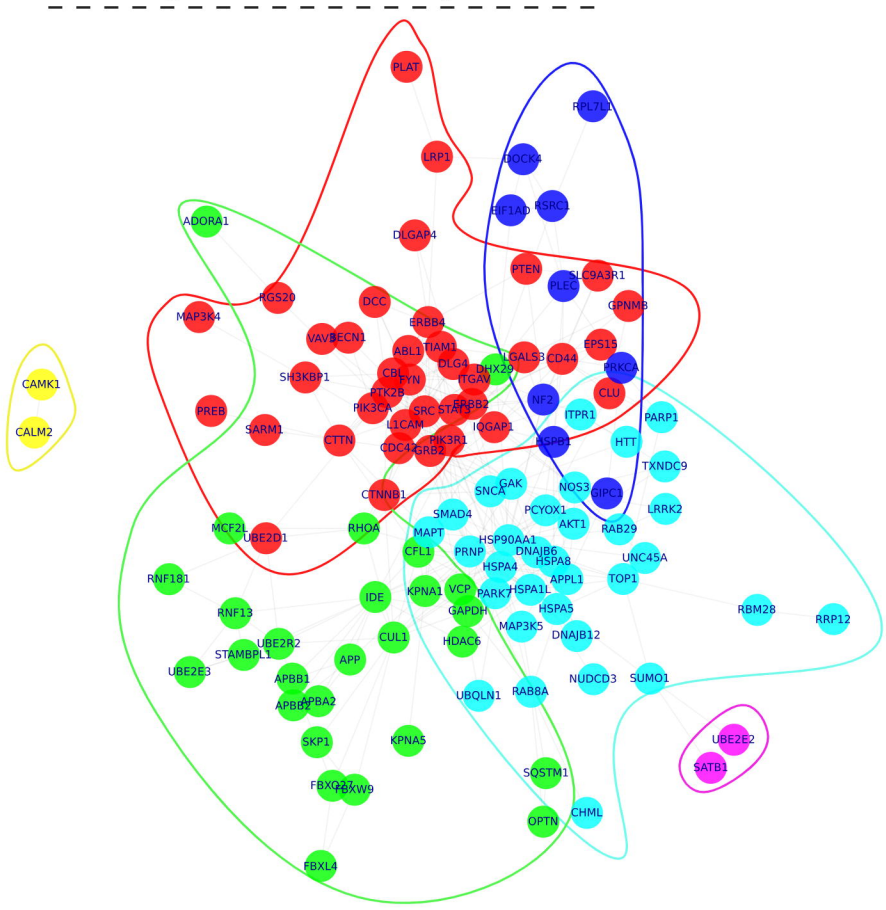

(B)

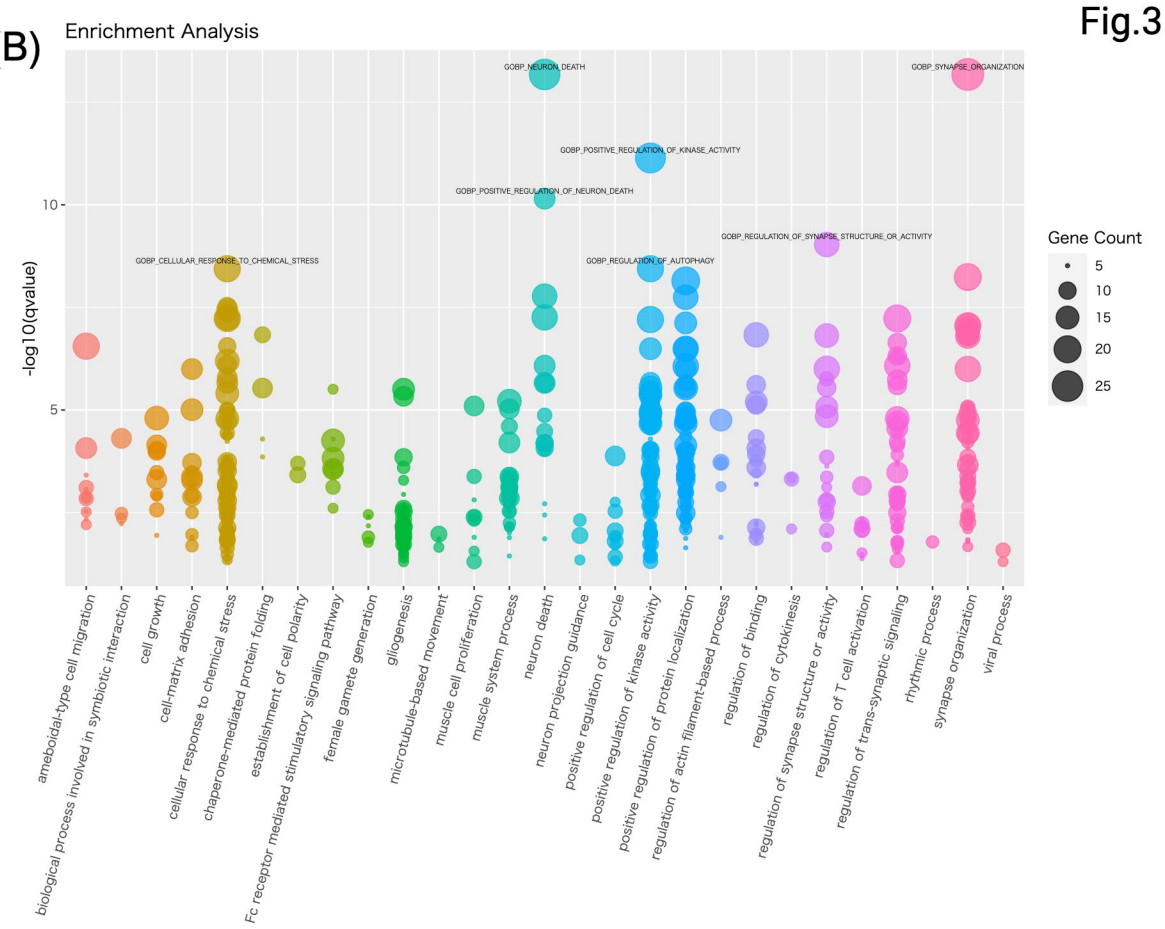

(C)

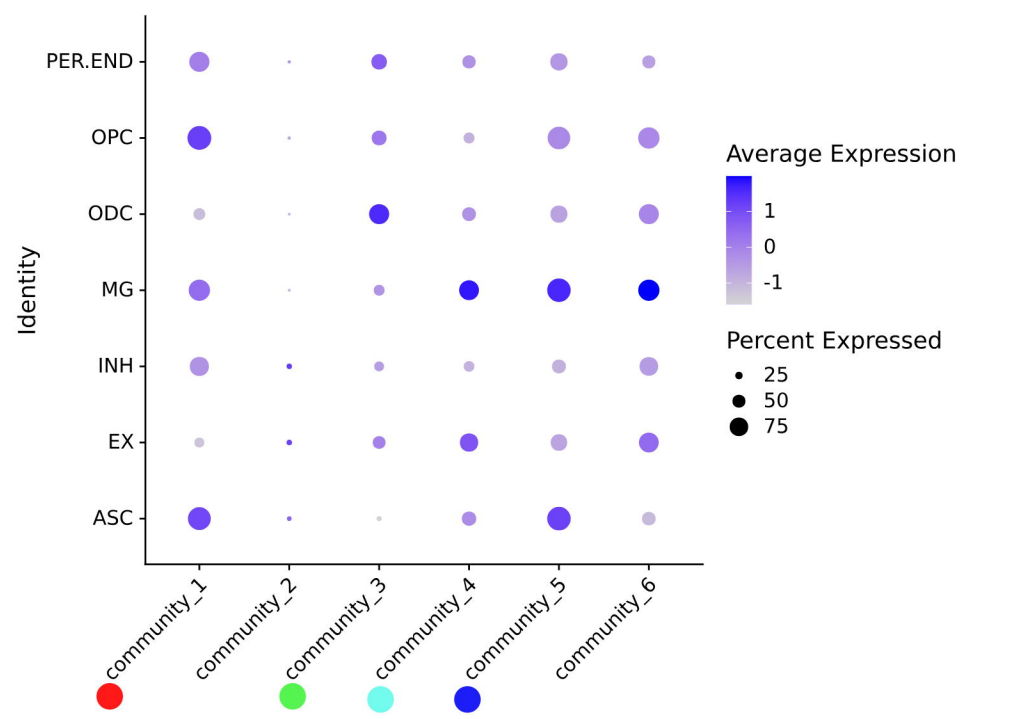

(D)

Fig.4

(A)

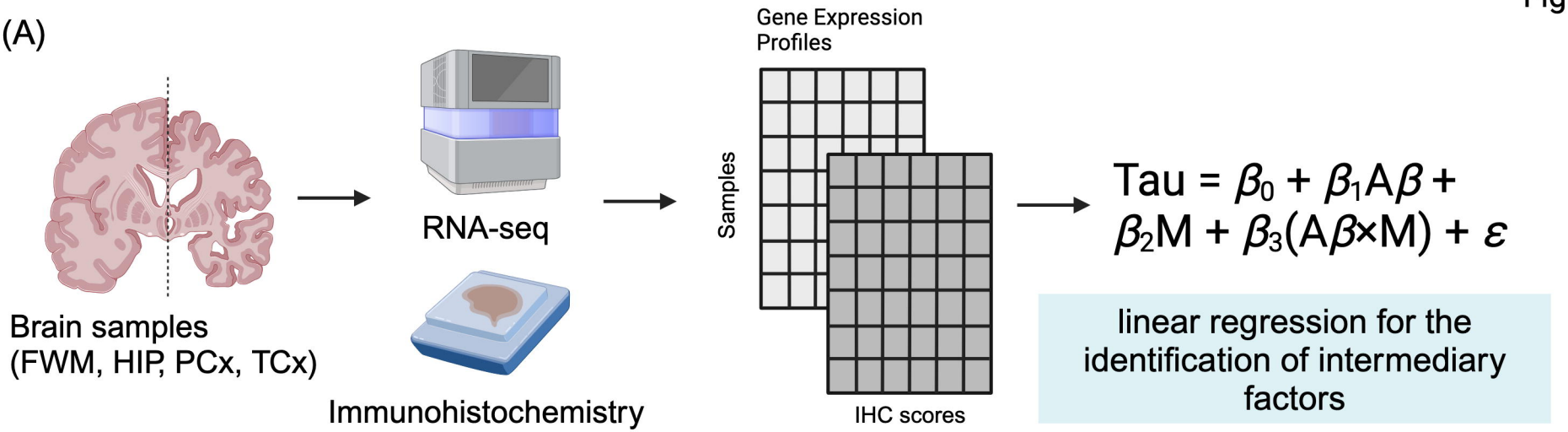
Brain samples
(FWM, HIP, PCx, TCx)
RNA-seq
Immunohistochemistry
Gene Expression Profiles
Samples
IHC scores
Tau = $\beta_0 + \beta_1 A\beta + \beta_2 M + \beta_3 (A\beta \times M) + \varepsilon$
linear regression for the identification of intermediary factors

(B)

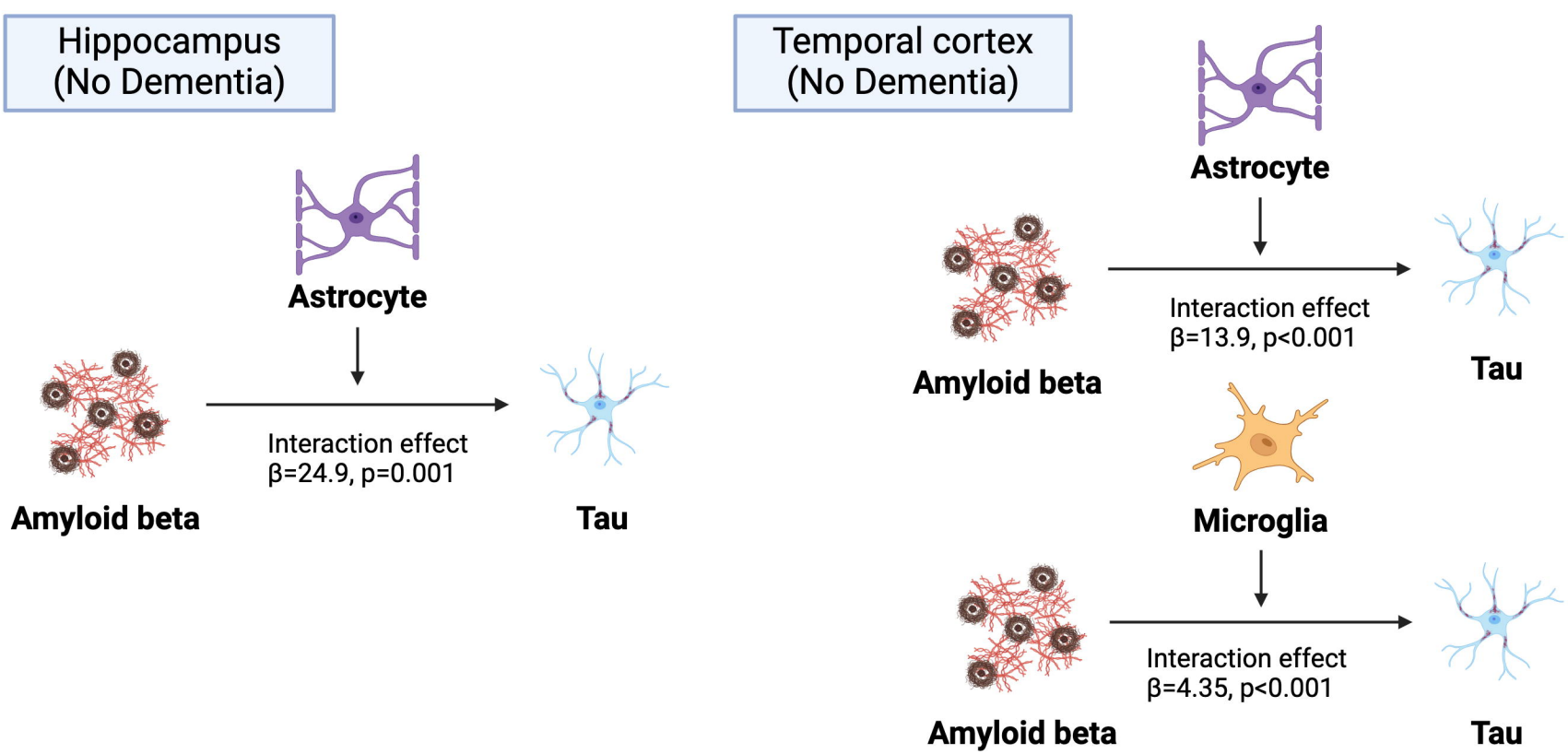
Hippocampus
(No Dementia)
Astrocyte
Amyloid beta
Interaction effect
β=24.9, p=0.001
Tau
Temporal cortex
(No Dementia)
Astrocyte
Amyloid beta
Interaction effect
β=13.9, p<0.001
Tau
Microglia
Amyloid beta
Interaction effect
β=4.35, p<0.001
Tau

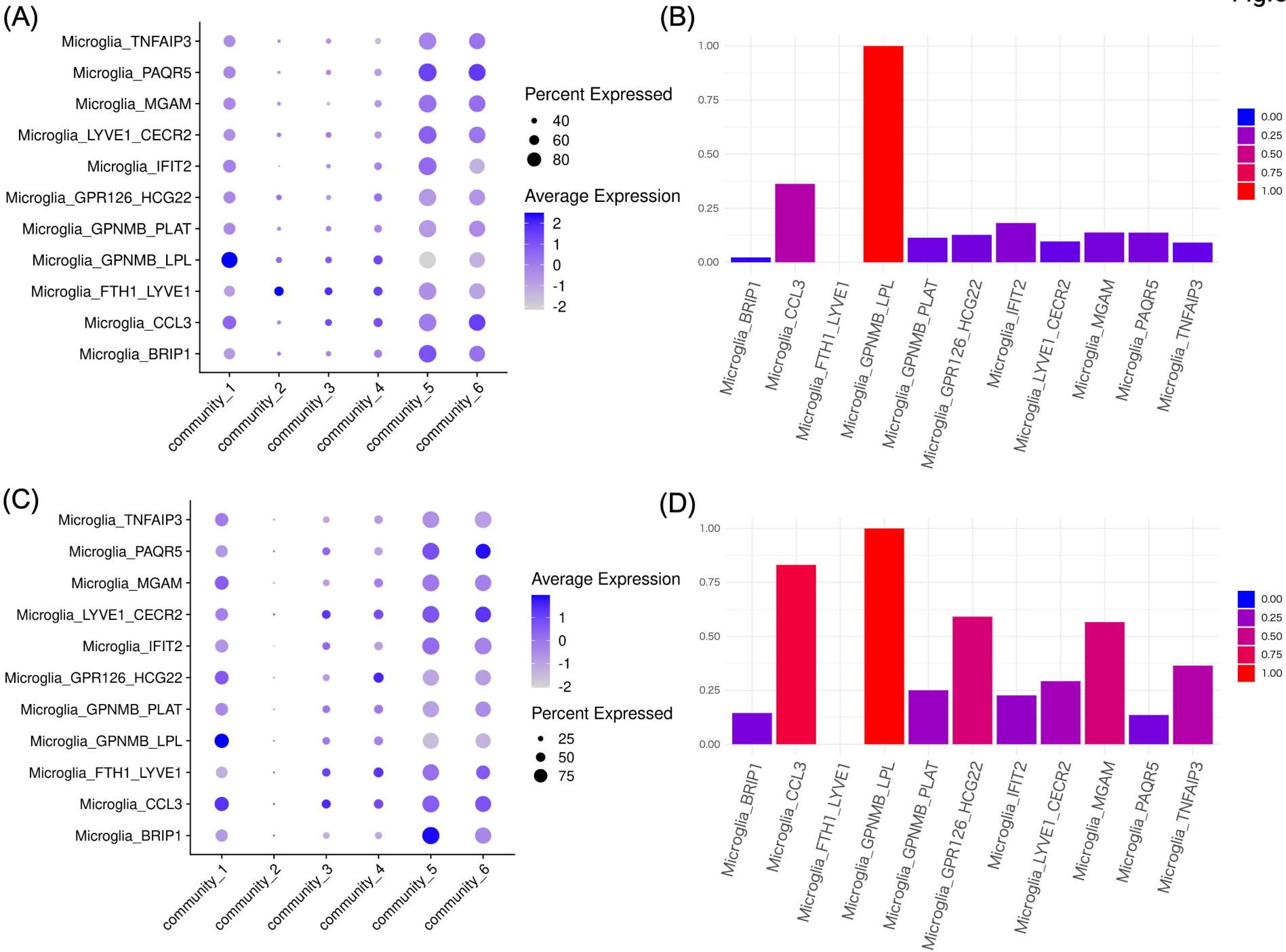
(A)
Microglia_TNFAIP3
Microglia_PAQR5
Microglia_MGAM
Microglia_LYVE1_CECR2
Microglia_IFIT2
Microglia_GPR126_HCG22
Microglia_GPNMB_PLAT
Microglia_GPNMB_LPL
Microglia_FTH1_LYVE1
Microglia_CCL3
Microglia_BRIP1
community_1
community_2
community_3
community_4
community_5
community_6
Percent Expressed
40
60
80
Average Expression
2
1
0
-1
-2
(B)
1.00
0.75
0.50
0.25
0.00
Microglia_BRIP1
Microglia_CCL3
Microglia_FTH1_LYVE1
Microglia_GPNMB_LPL
Microglia_GPNMB_PLAT
Microglia_GPR126_HCG22
Microglia_IFIT2
Microglia_LYVE1_CECR2
Microglia_MGAM
Microglia_PAQR5
Microglia_TNFAIP3
0.00
0.25
0.50
0.75
1.00
(C)
Microglia_TNFAIP3
Microglia_PAQR5
Microglia_MGAM
Microglia_LYVE1_CECR2
Microglia_IFIT2
Microglia_GPR126_HCG22
Microglia_GPNMB_PLAT
Microglia_GPNMB_LPL
Microglia_FTH1_LYVE1
Microglia_CCL3
Microglia_BRIP1
community_1
community_2
community_3
community_4
community_5
community_6
Average Expression
1
0
-1
-2
Percent Expressed
25
50
75
(D)
1.00
0.75
0.50
0.25
0.00
Microglia_BRIP1
Microglia_CCL3
Microglia_FTH1_LYVE1
Microglia_GPNMB_LPL
Microglia_GPNMB_PLAT
Microglia_GPR126_HCG22
Microglia_IFIT2
Microglia_LYVE1_CECR2
Microglia_MGAM
Microglia_PAQR5
Microglia_TNFAIP3
0.00
0.25
0.50
0.75
1.00

Fig.6

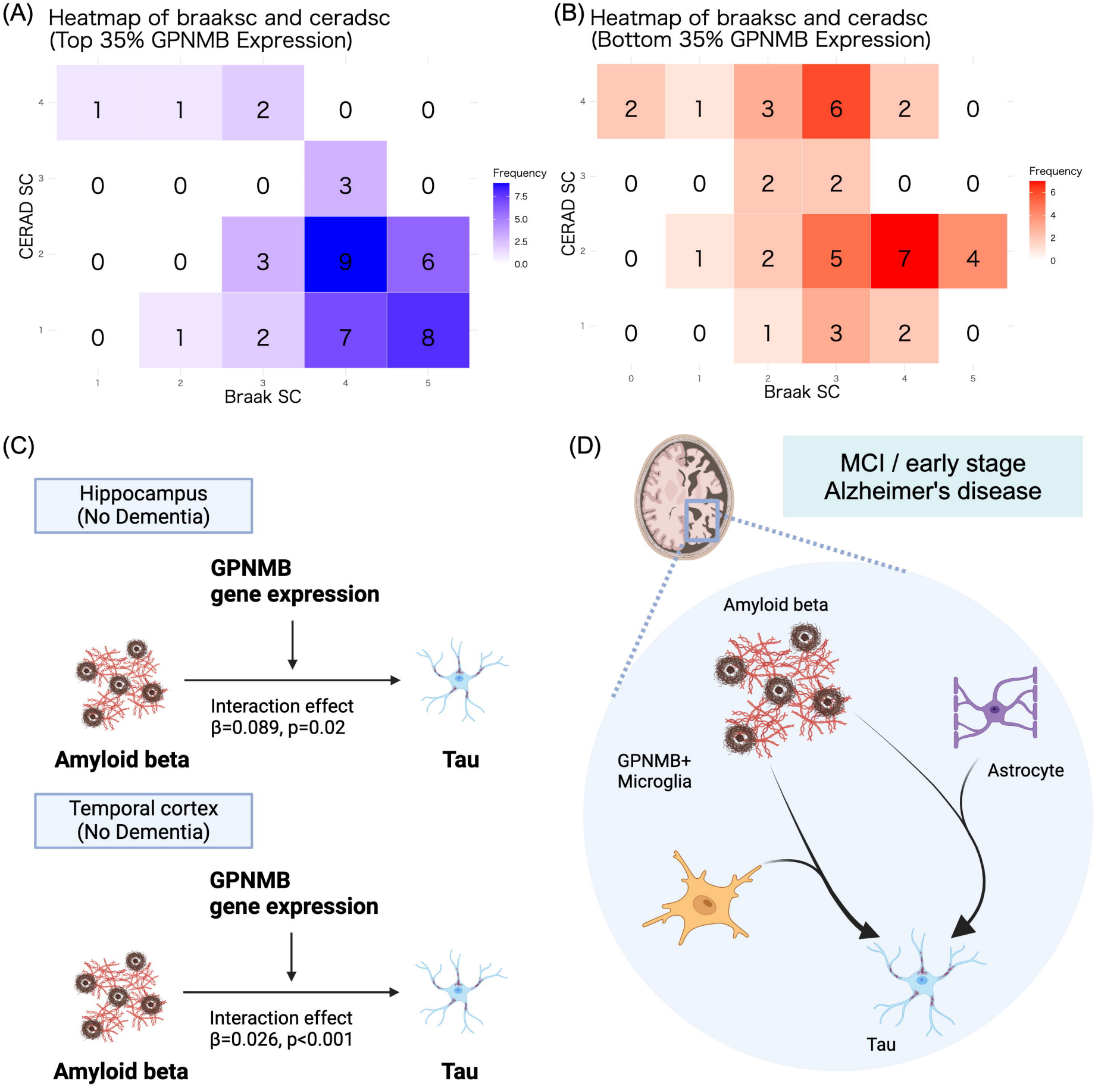
(A)
Heatmap of braaksc and ceradsc
(Top 35% GPNMB Expression)
CERAD SC
Braak SC
Frequency
7.5
5.0
2.5
0.0
(B)
Heatmap of braaksc and ceradsc
(Bottom 35% GPNMB Expression)
CERAD SC
Braak SC
Frequency
(C)
Hippocampus
(No Dementia)
GPNMB
gene expression
Interaction effect
β=0.089, p=0.02
Amyloid beta
Tau
Temporal cortex
(No Dementia)
GPNMB
gene expression
Interaction effect
β=0.026, p<0.001
Amyloid beta
Tau
(D)
MCI / early stage
Alzheimer's disease
Amyloid beta
GPNMB+
Microglia
Astrocyte
Tau

Supplementary Fig.S1

Study design

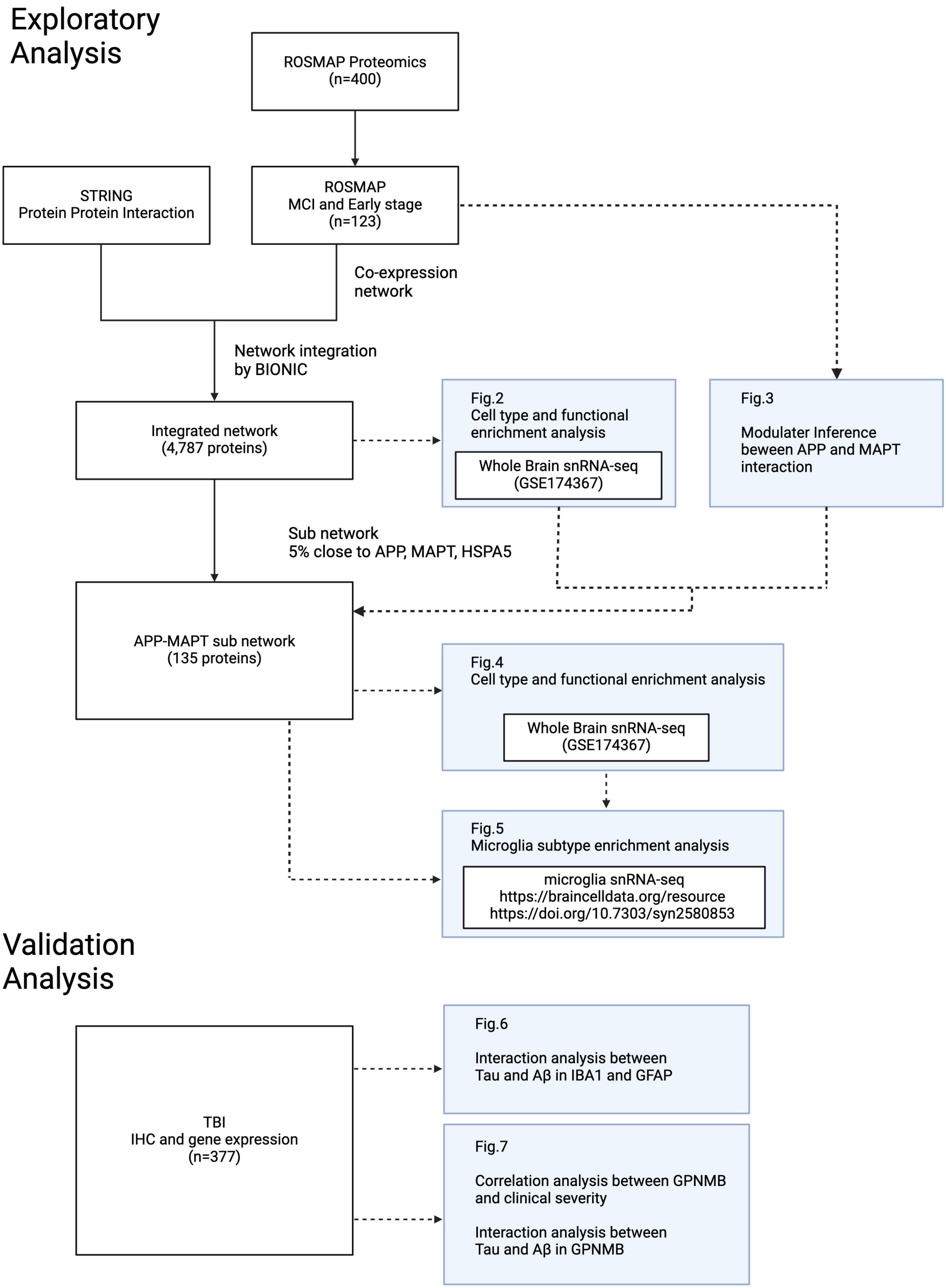

Supplementary Fig.S2

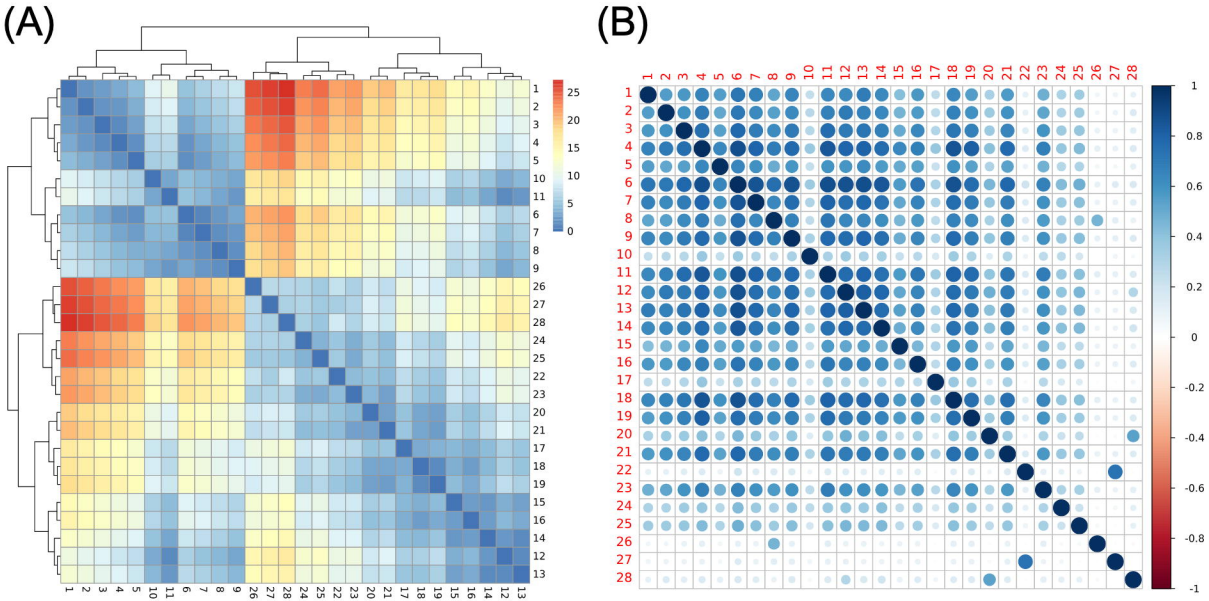

Supplementary Fig.S3

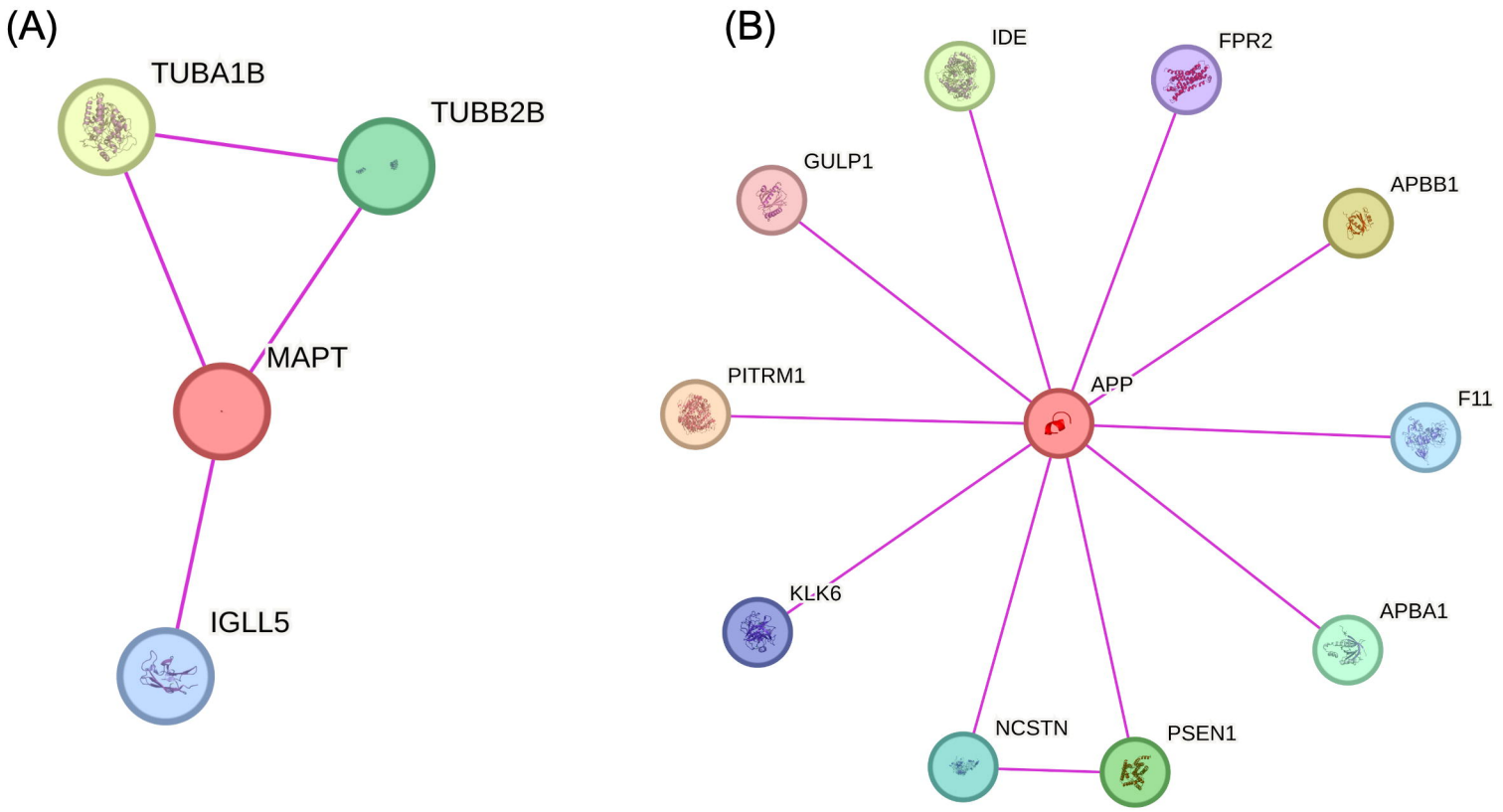

Supplementary Fig.S4

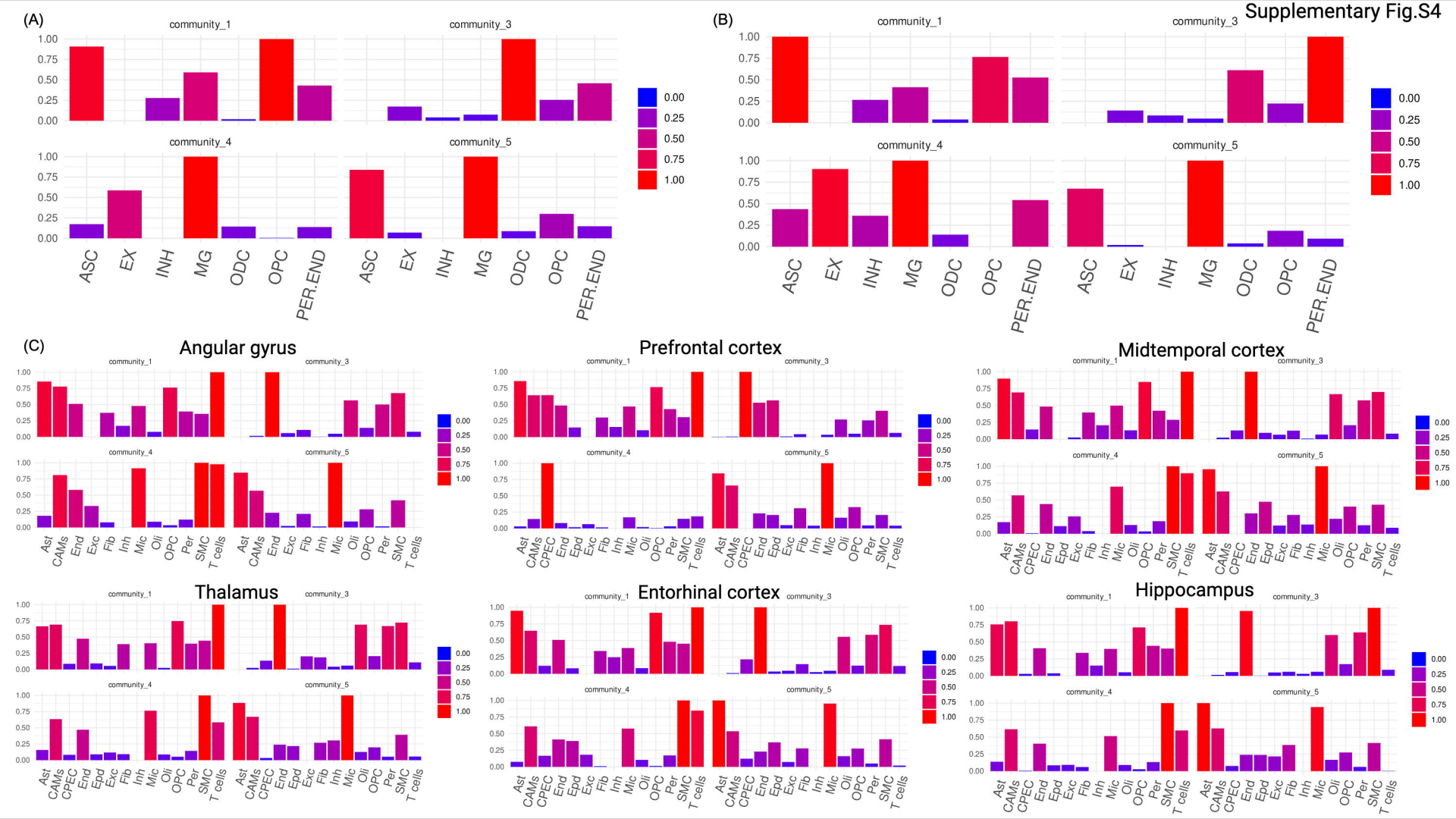

Supplementary Fig.S5

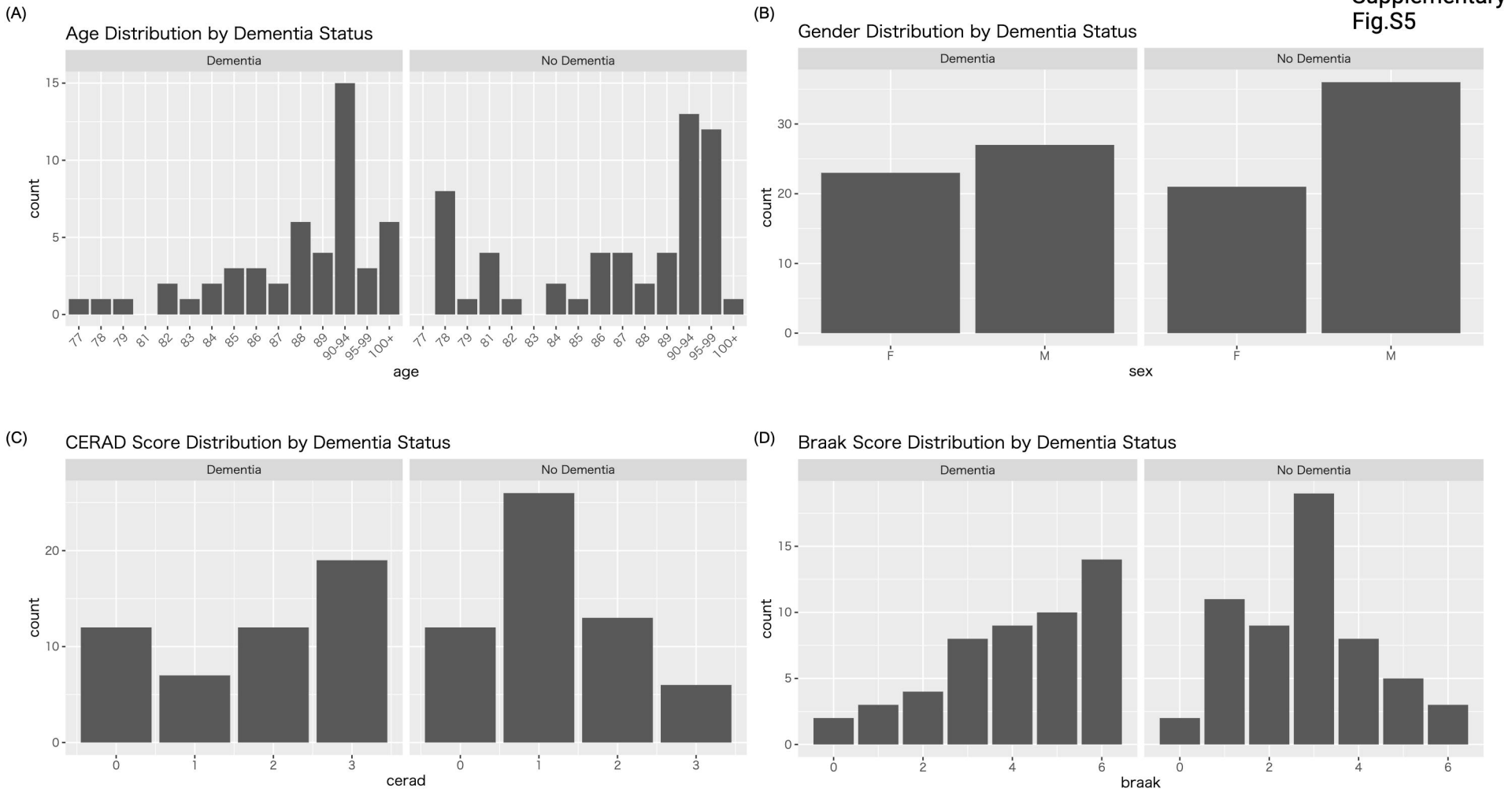

Supplementary Fig.S6

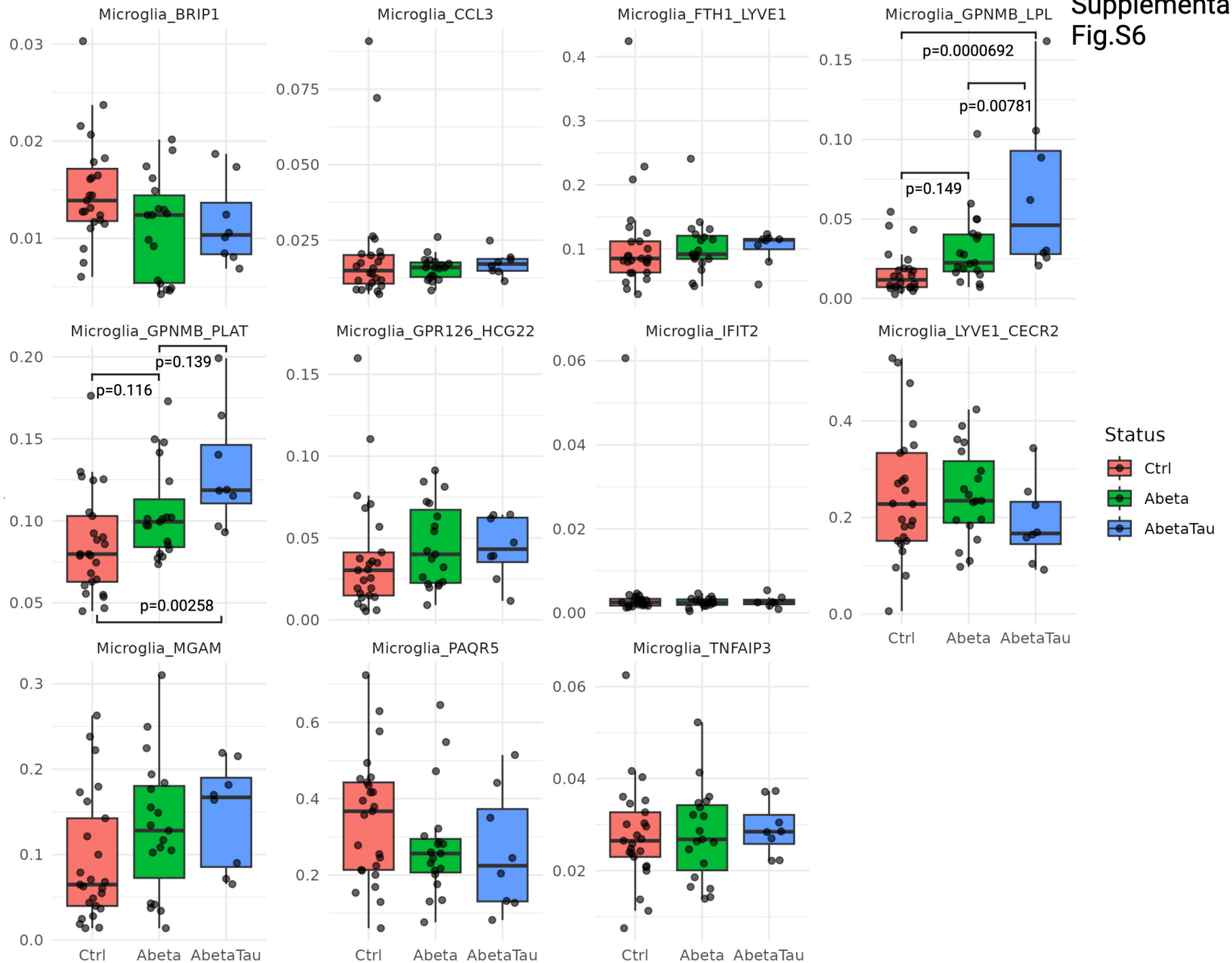
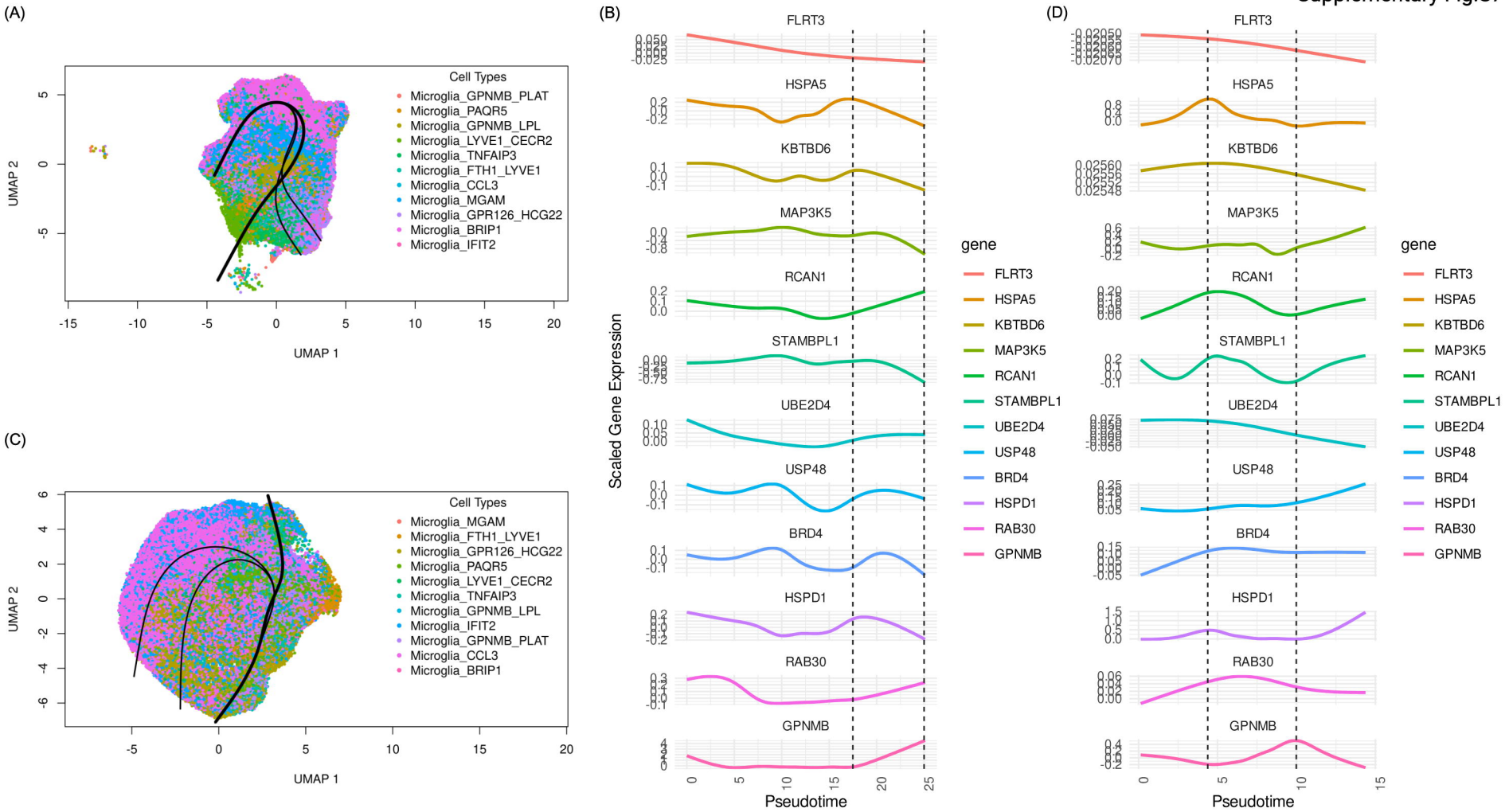
Supplementary Fig.S7